REPORT DOCUMENTATION PAGE

1a. REPORT SECURITY CLASSIFICATION: UNCLASSIFIED	1b. RESTRICTIVE MARKINGS
2a. SECURITY CLASSIFICATION AUTHORITY	3. DISTRIBUTION/AVAILABILITY OF REPORT: Approved for public release; distribution is unlimited
2b. DECLASSIFICATION/DOWNGRADING SCHEDULE	
4. PERFORMING ORGANIZATION REPORT NUMBER(S): CR 88-01	5. MONITORING ORGANIZATION REPORT NUMBER(S): CR 88-01
6a. NAME OF PERFORMING ORGANIZATION: Dept, of Atmospheric Sciences University of Washington; 6b. OFFICE SYMBOL (If applicable): AK-40	7a. NAME OF MONITORING ORGANIZATION: Naval Environmental Prediction Research Facility
6c. ADDRESS (City, State, and ZIP Code): Seattle, WA 98195	7b. ADDRESS (City, State, and ZIP Code): Monterey, CA 93943-5006
8a. NAME OF FUNDING/SPONSORING ORGANIZATION: Office of Naval Research; 8b. OFFICE SYMBOL (If applicable): ONT	9. PROCUREMENT INSTRUMENT IDENTIFICATION NUMBER: N00014-86-K-0453
8c. ADDRESS (City, State, and ZIP Code): 800 N. Quincy St. Arlington, VA 22217	10. SOURCE OF FUNDING NUMBERS: PROGRAM ELEMENT NO. 62435N; PROJECT NO. R3582; TASK NO.; WORK UNIT ACCESSION NO. DN656759

11. TITLE (Include Security Classification): Passive Microwave Measurements of Water Vapor Fields and Rain for Locating Fronts in Cyclonic Storms (U)

12. PERSONAL AUTHOR(S): Katsaros, Kristina B.; Bhatti, Iftekhar A.; McMurdie, Lynn A.; and Petty, Grant W.

13a. TYPE OF REPORT	13b. TIME COVERED	14. DATE OF REPORT (Year, Month, Day)	15. PAGE COUNT
Final	FROM 7/1/86 TO 8/31/87	1988, March	50

16. SUPPLEMENTARY NOTATION

17. COSATI CODES			18. SUBJECT TERMS (Continue on reverse if necessary and identify by block number)
FIELD	GROUP	SUB-GROUP	Satellite, Microwave, Fronts, Precipitation, Precipitable water
04	01		

19. ABSTRACT (Continue on reverse if necessary and identify by block number)

This report describes some basic research techniques and algorithms developed to diagnose fronts in cyclonic storms over the ocean with passive microwave data. The need for this research stems from the limited availability of reliable weather reports over the ocean, and the occasional disruption of weather map transmissions.

In earlier work we found that strong gradients in integrated atmospheric water vapor are good indicators of surface locations of fronts in midlatitude cyclones over the oceans. A second significant indicator of frontal activity is precipitation. Therefore, we have developed methods for flagging strong gradients in integrated atmospheric water vapor (WVG-flag) and the presence of rain by using data from the Scanning Multichannel Microwave Radiometer (SMMR) aboard polar-orbiting Seasat and Nimbus-7 satellites. The data were not received in real time, but were analyzed from archived tapes. Examination of 65 frontal systems showed the water vapor gradient flag to catch 86% of the fronts while the

((continued on reverse))

20. DISTRIBUTION/AVAILABILITY OF ABSTRACT: ☒ UNCLASSIFIED/UNLIMITED ☐ SAME AS RPT ☐ DTIC USERS	21. ABSTRACT SECURITY CLASSIFICATION: UNCLASSIFIED
22a. NAME OF RESPONSIBLE INDIVIDUAL: Dr. Paul M. Tag, contract monitor	22b. TELEPHONE (Include Area Code): (408) 647-4737; 22c. OFFICE SYMBOL: NEPRF WU 6.2-9

Block 19, Abstract, continued

precipitation flagged 90%. Each flag emphasizes different portions of the cyclone and are therefore complimentary.

Ultimately these techniques are intended for operational use with data from the Special Sensor Microwave Imager (SSM/I) which was launched in June 1987 on a satellite in the Defense Meteorological Satellite Program (DMSP). Such data can be received in real time directly by ships at sea.

AN (1) AD-A195 632
FG (2) 040200
CI (3) (U)
CA (5) WASHINGTON UNIV SEATTLE DEPT OF ATMOSPHERIC SCIENCES
TI (6) Passive Microwave Measurments of Water Vapor Fields and Rain for Locating Fronts in Cyclonic Storms.
TC (8) (U)
DN (9) Final rept. 1 Jul 86-31 Aug 87,
AU (10) Katsaros, Kristina B.
AU (10) Bhatti, Iftekhar A.
AU (10) McMurdie, Lynn A.
AU (10) Petty, Grant W.
RD (11) Mar 1988
PG (12) 50
CT (15) N00014-86-K-0453
PJ (16) R3582
RN (18) NEPRF-CR-88-01
RC (20) Unclassified report
DE (23) *CYCLONES, *MICROWAVE EQUIPMENT, *MICROWAVES, *RADIOMETERS, *WEATHER, ALGORITHMS, AVAILABILITY, DEPARTMENT OF DEFENSE, DETECTORS, IMAGES, INDICATORS, METEOROLOGICAL SATELLITES, MULTICHANNEL, OCEANS, PASSIVE SYSTEMS, POSITION(LOCATION), PRECIPITATION, RAIN, REAL TIME, RELIABILITY, REPORTS, SCANNING, SEA BASED, SHIPS, STORMS, SURFACES, WATER VAPOR.
DC (24) (U)
ID (25) PE62435N, WUDN656759.
IC (26) (U)
AB (27) This report describes some basic research techniques and algorithms developed to diagnose fronts in cyclonic storms over the ocean with passive microwave data. The need for this research stems from the limited availability of reliable weather reports over the ocean, and the occasional disruption of weather map transmissions. In earlier work we found that strong gradients in integrated atmospheric water vapor are good indicators of surface locations of fronts in midlatitude cyclones over the oceans. A second significant indicator of frontal activity is precipitation. Therefore, we have developed methods for flagging strong gradients in integrated atmospheric water vapor (WVG-flag) and the presence of rain by using data from the Scanning Multichannel Microwave Radiometer (SMMR) aboard polar-orbiting Seasat and Nimbus-7 satellites. The data were not received in real time, but were analyzed from archived tapes. Examination of 65 frontal systems showed the water vapor gradient flag to catch 86% of the fronts while the precipitation flagged 90%. Each flag emphasizes different portions of the cyclone and are therefore complimentary. Ultimately these techniques are intended for operational use with data from the Special Sensor

Microwave Imager (SSM/I) which was launched in June 1987 on a satellite in the Defense Meteorological Satellite Program (DMSP). Such data can be received in real time directly by ships at sea. (RH)
AC (28) (U)
DL (33) 01

SE (34) F
CC (35) 370270

#

ROUTINE REPLY, ENDORSEMENT, TRANSMITTAL OR INFORMATION SHEET

OPNAV 5216/158 (Rev. 7-78) *A WINDOW ENVELOPE MAY BE USED*
SN 0107-LF-052-1691 *Formerly NAVEXOS 3789*

CLASSIFICATION (*UNCLASSIFIED when detached from enclosures, unless otherwise indicated*) UNCLASSIFIED

FROM (*Show telephone number in addition to address*)
Commanding Officer, Naval Environmental Prediction Research Facility, Monterey, CA 93943-5006 AV 878-4731

DATE
23 May 88

SUBJECT
FORWARDING OF NAVENVPREDRSCHFAC TECHNICAL PUBLICATION

SERIAL OR FILE NO.
5600 NEPRF/SBB:sb
Ser 186

TO:
Distribution
[Encl (1), pp 44, 45]

REFERENCE

ENCLOSURE
(1) NAVENVPREDRSCHFAC Contractor Report CR 88-01; Passive Microwave Measurements of Water Vapor Fields and Rain for Locating Fronts in Cyclonic Storms

VIA:

ENDORSEMENT ON

[X] FORWARDED [ ] RETURNED [ ] FOLLOW-UP, OR TRACER [ ] REQUEST [ ] SUBMIT [ ] CERTIFY [ ] MAIL [ ] FILE

GENERAL ADMINISTRATION		CONTRACT ADMINISTRATION		PERSONNEL	
	FOR APPROPRIATE ACTION		NAME & LOCATION OF SUPPLIER OF SUBJECT ITEMS		REPORTED TO THIS COMMAND:
	UNDER YOUR COGNIZANCE		SUBCONTRACT NO. OF SUBJECT ITEM		
X	INFORMATION & retention		APPROPRIATION SYMBOL, SUBHEAD, AND CHARGEABLE ACTIVITY		DETACHED FROM THIS COMMAND
	APPROVAL RECOMMENDED [ ] YES [ ] NO		SHIPPING AT GOVERNMENT EXPENSE [ ] YES [ ] NO		
	[ ] APPROVED [ ] DISAPPROVED		A CERTIFICATE, VICE BILL OF LADING		OTHER
	COMMENT AND/OR CONCURRENCE		COPIES OF CHANGE ORDERS, AMENDMENT OR MODIFICATION		
	CONCUR		CHANGE NOTICE TO SUPPLIER		
	LOANED, RETURN BY:		STATUS OF MATERIAL ON PURCHASE DOCUMENT		
	SIGN RECEIPT & RETURN				
	REPLY TO THE ABOVE BY:				
	REFERENCE NOT RECEIVED				
	SUBJECT DOCUMENT FORWARDED TO:				
	SUBJECT DOCUMENT RETURNED FOR:				
	SUBJECT DOCUMENT HAS BEEN REQUESTED, AND WILL BE FORWARDED WHEN RECEIVED				
	COPY OF THIS CORRESPONDENCE WITH YOUR REPLY				
	ENCLOSURE NOT RECEIVED				
	ENCLOSURE FORWARDED AS REQUESTED				
	ENCLOSURE RETURNED FOR CORRECTION AS INDICATED				
	CORRECTED ENCLOSURE AS REQUESTED				
	REMOVE FROM DISTRIBUTION LIST				
	REDUCE DISTRIBUTION AMOUNT TO:				

REMARKS (*Continue on reverse*)

Enclosure (1) describes some basic research techniques and algorithms that have been developed to diagnose fronts in cyclonic storms over the ocean using data gathered by passive microwave sensors.

SIGNATURE & TITLE
Wayne S. Shiver
WAYNE S. SHIVER, By direction

COPY TO:

CLASSIFICATION (*UNCLASSIFIED when detached from enclosures, unless otherwise indicated*) UNCLASSIFIED

★ G.P.O.: 1982-587-016/5340

Naval Environmental Prediction Research Facility
Monterey, CA 93943-5006

Contractor Report | CR 88-01 | March 1988

PASSIVE MICROWAVE MEASUREMENTS OF WATER VAPOR FIELDS AND RAIN FOR LOCATING FRONTS IN CYCLONIC STORMS

K.B. Katsaros, I.A. Bhatti,
L.A. McMurdie, G.W. Petty
University of Washington
Seattle, WA 98195

CONTENTS

1. INTRODUCTION

1.1 Purpose and Motivation for the Project

This project is designed to document some basic research techniques and algorithms developed to diagnose fronts in cyclonic storms over the ocean using passive microwave data. These techniques and algorithms have been developed using data from the Scanning Multichannel Microwave Radiometers (SMMR's) on the polar orbiting Seasat and Nimbus 7 satellites. Ultimately these techniques are intended for operational use with data from the Special Sensor Microwave Imager (SSM/I) which was launched in June 1987 on a satellite in the Defense Meteorological Satellite Program (DMSP). Such data can be received in real time directly by ships at sea. The need for this research stems from the limited availability of reliable weather reports over the ocean, and the occasional disruption of weather map transmissions.

1.2 Specific Goals Covered in this Report

The goal of the work described in this report is to devise an operational method for flagging strong gradients in integrated atmospheric water vapor obtained from the data collected with the SMMR. In earlier work we have found that these gradients are good indicators of the surface location of fronts in midlatitude cyclones over oceans.

A second indicator of frontal activity is precipitation. The presence of rain can also be flagged with SMMR data. The statistical reliability of these indicators of frontal location is also presented.

2. BACKGROUND

2.1 Relation between Passive Microwave Data and Cyclones

Ocean-atmosphere interaction plays an important role in cyclogenesis. The initiation and development of cyclones often occur over the ocean. However, the sparsity of data in these regions severely inhibits the study and forecasting of these storms. In the last 20 years, satellite-borne instruments have begun to alleviate this problem. Visible and infrared satellite images have been very useful in identifying cloud systems associated with mid-latitude cyclones, and they have improved our ability to locate surface fronts and upper level features (e.g., Anderson, et al., 1969). The passive microwave data obtained from the two microwave radiometers, the SMMR's, on Seasat and

Nimbus 7 were not received in real time, but were analyzed from archived tapes. Over the oceans the following atmospheric and surface parameters can be obtained from the SMMR's: sea surface temperature, surface wind speed, integrated water vapor, sea ice and rain rate (Gloersen, et al., 1984). The horizontal distribution of integrated water vapor is well suited for locating fronts (McMurdie and Katsaros, 1985; Katsaros and Lewis, 1986) and the patterns were found to be well correlated with surface convergence derived from the Seasat scatterometer (McMurdie, et al., 1987). For the relatively low intensity, wide-spread rain of mid-latitude cyclones, the areally-averaged rain rates estimated from the SMMR's show qualitative agreement with ship observations and coastal rain gauges (McMurdie and Katsaros, 1985; Katsaros and Lewis, 1986). The main results of these studies relevant to the present work are:

a) The surface cold front in a midlatitude cyclone over the ocean is typically located near the leading edge of a strong gradient in integrated water vapor.

b) The rain rate algorithms provide rain rates within some rather large error margins (factor of 2 or 3 or more). The identification of areas with rain in midlatitude cyclones seems to be very good.

c) Wind speeds derived from Nimbus 7 data outside rain areas, are in good agreement with in situ buoy or ship data.

The assertions made under a) and b) were based on data in the Northern Hemisphere from Seasat SMMR, which was limited to the late summer, early fall season. Therefore our first task was to examine whether the assertions made under a), and b), above, are generally valid in different parts of the world ocean including the southern hemisphere, and in different seasons. We studied North Pacific winter storms, which occurred during the Storm Transfer and Response Experiment (STREX, Fleagle et al., 1982) and several storms during 1979, which was the first year of Nimbus 7 operation, and which also coincided with the First GARP Global Experiment (FGGE). Good comparison data are therefore available for that year. In an interim technical report under this contract (Katsaros, et al., 1987) we demonstrated that these assertions were true. We have now increased our data base further by adding about 20 rapidly deepening cyclones.

The patterns of water vapor derived from these algorithms are striking verification of the Norwegian Model of cyclonic storms (e.g., Bjerknes, 1919; Bjerknes and Solberg, 1922). Figure 2.1 shows examples of how the pattern of integrated water vapor relates to the surface location of an atmospheric cold front.

2.2 The Characteristics of the Scanning Multichannel Microwave Radiometer and of the Special Sensor Microwave Imager

The design of the Scanning Multichannel Microwave Radiometer was based on more than a decade of development of passive microwave radiometry (Gloersen and Barath, 1977). It has five frequencies of varying resolution and varying sensitivity to a multitude of geophysical parameters. In Table 2.1 the parameters sensed by the three highest frequencies are the ones needed for analysis of atmospheric water.

TABLE 2.1: CHARACTERISTICS OF THE NIMBUS 7 SMMR

Frequency GHZ	Resolution km x km	Geophysical Parameters of Interest
6.6	156 x 158	Sea surface temperature
10.7	98 x 98	Surface wind speed
18.0	60 x 60	Integrated cloud liquid water and rain
21.0	60 x 60	Integrated water vapor
37.0	30 x 30	Rain size droplets and cloud water

High emissivity of land surfaces obscures the cloud, rain and water vapor emissions; therefore, satellite passes over land are not usable for the analysis of cyclonic storms. The ocean surface on the other hand, with its low emissivity and relatively uniform brightness temperature provides an excellent background for observing the atmospheric water vapor, cloud and rain water. The 21 GHZ channel is in a weak absorption band of atmospheric water vapor which does not saturate even over tropical oceans. It is therefore possible to measure the total integrated amount of water vapor (often called precipitable water) when measuring over a relatively constant background such as the ocean surface. Cloud and rain droplets produce enhanced signals at 18 and 37 GHz by Rayleigh and Mie scattering and emission. At the intermediate wavelength of 21 GHz, the emission of the water vapor gas

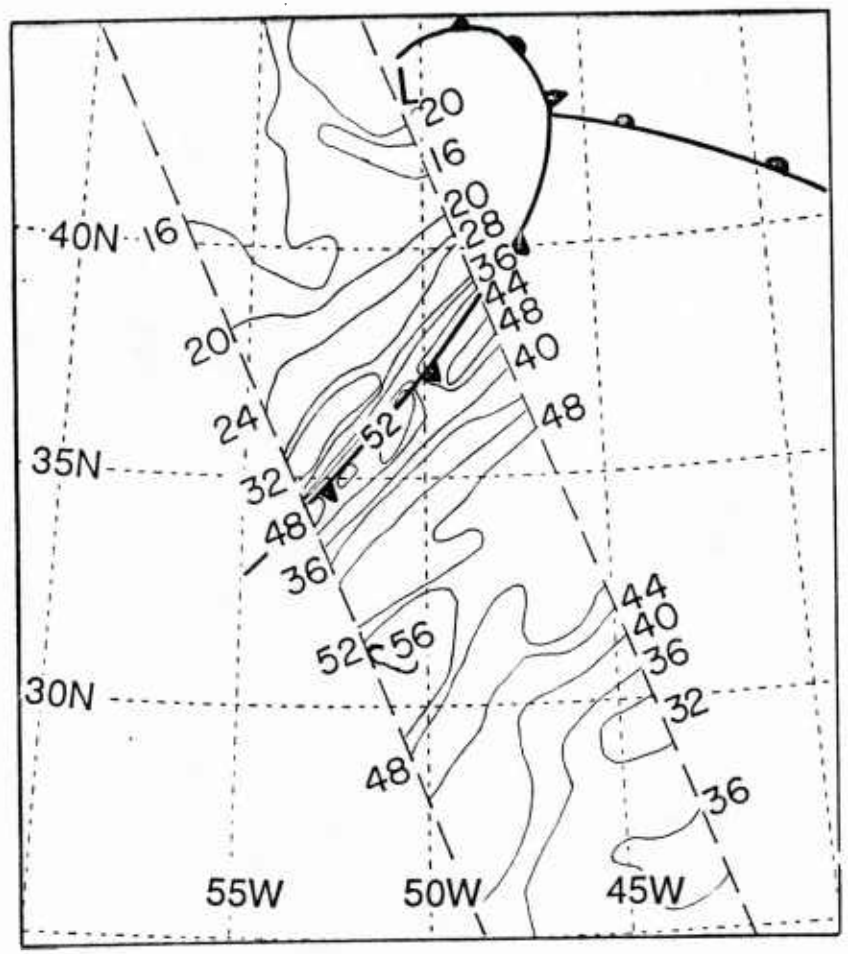

(a) Integrated water vapor in kg m^{-2}

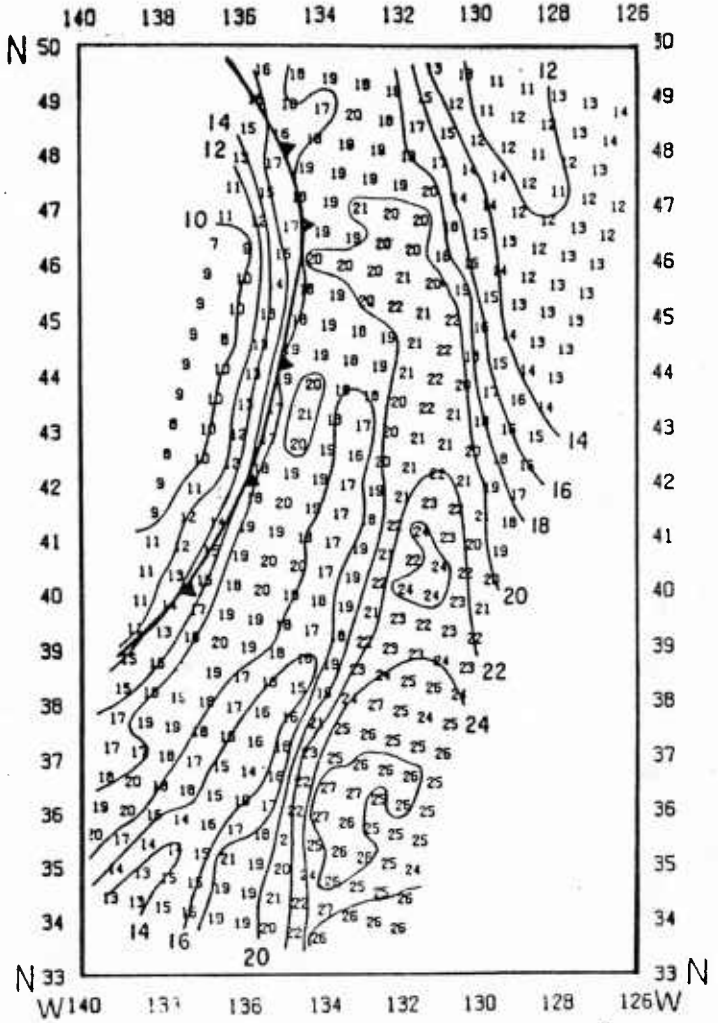

(b) Integrated water vapor in kg m^{-2}

Figure 2.1 Examples of integrated water vapor patterns obtained with the SMMR's and their relation to the surface location of cold fronts. Values are in kg m^{-2}. The location of the fronts have been determined by independent analysis.

a) Data from Seasat for the Queen Elizabeth II Storm over the Gulf Stream (after McMurdie et al., 1987).

b) Data from Nimbus 7 off the West Coast of the U.S.A. for March 17, 1979 at 01:16 GMT, Orbit #1992 (after Katsaros and Lewis, 1986).

dominates and corrections for interference by cloud and rain droplets have to be made. In very heavy rain this correction fails, so that the water vapor algorithm becomes invalid. Algorithms for interpreting the 18 and 37 GHz brightness temperatures in terms of rain rate have been developed based on models of radiative transfer (e.g., Wilheit and Chang, 1980), but verification is limited.

The SMMR's swath width on Nimbus 7 was 800 km, while on the Seasat satellite it was 600 km. The Seasat SMMR's resolution is slightly greater. Each overpass is translated by about 26° of longitude from the previous pass. Typically, it is not possible for SMMR to view a whole storm in one pass because the storm covers a much larger area than a swath. A storm can be overlooked altogether if it fits between two overpasses. Sometimes it is possible to sample the storm at several stages and in different sectors with data from several overpasses over 24 to 48 hour periods. Unfortunately, the Nimbus 7 SMMR was operated on alternate days, which makes it impossible to follow the development of a storm system in detail. With the Seasat SMMR we had continuous coverage, but this satellite terminated prematurely after a lifetime of only three months.

As mentioned, in the future we are planning to use data obtained with the SSM/I. The SSM/I is a microwave radiometer with channels at 19.3, 22.2, 37 and 85.5 GHz. The three lower frequencies have similar responses to atmospheric water as the 18, 21 and 37 GHz channels on the SMMR's and the surface resolution is comparable. Thus, the findings we report here should have application to SSM/I data with only minor modifications. The swath width is 1394 km, about twice that of the SMMR's and the instrument is "on" continuously, providing much better sampling of cyclones with passive microwave data than we have seen to date.

3. METHODS OF ANALYSIS

Using passive microwave data from the 18, 21 and 37 GHz channels on the two satellite-borne SMMR's, we have studied the patterns of integrated atmospheric water vapor and rain rate.

3.1 Algorithms Used to Calculate Atmospheric Water Vapor

The User's Guides for the SMMR's on Seasat and Nimbus 7 provide guidance for calculating the integrated atmospheric water vapor. (SMMR Mini-Workshop IV Report, 1981; Seasat Geophysical Data Record User's Handbook, 1982; and User's Guide for the Nimbus 7 SMMR PARM and MAP Tapes, 1983.) We have mostly used Nimbus 7 SMMR data in this study. Its algorithms are based on the work of Staelin et al. (1976), Rosenkranz et al. (1978) and Chang and Wilheit (1979). This algorithm is found in Appendix A. Because of a deterioration with time of the 21 GHz channel (horizontal polarization), corrections to the brightness temperature outlined by Kim et al. (1985) had to be applied. The integrated water vapor values obtained from two SMMR instruments have been found to be in excellent agreement with values obtained by integrating the data from radiosonde ascents (Katsaros, et al., 1981; Alishouse, 1983; Gloersen, et al., 1984; and Prabhakara, et al., 1982). Our own tests of the accuracy of the Nimbus 7 SMMR is found in Figure 3.1.

3.2 Smoothing and Gradient Algorithms

Because we consistently found the surface location of cold fronts to be ahead of the strongest gradient, or at the leading edge of it in integrated atmospheric water vapor, with the maximum water vapor lying ahead of the cold front, we decided to calculate the gradient perpendicular to the contours, and to flag values greater than a certain number. These flags would then indicate the general vicinity of the front. In order to eliminate spurious large gradient values associated with "spikes" in the retrieved water vapor field, we first apply a smoothing routine.

Smoothing Algorithm: Water vapor values computed for each element of a 13 by 13 matrix of gridded SMMR measurements are smoothed using a median filter. The method consists of replacing each grid value with the median of the values contained in a 3 by 3 pixel window centered on the pixel to be adjusted. This value represents the median of nine values in the center of the array, fewer on the edges of the grid.

Gradient Algorithm: First, gradient components are computed for the along-swath and cross-swath directions by taking the difference of the values on either side of the pixel for which the gradient is being computed and dividing

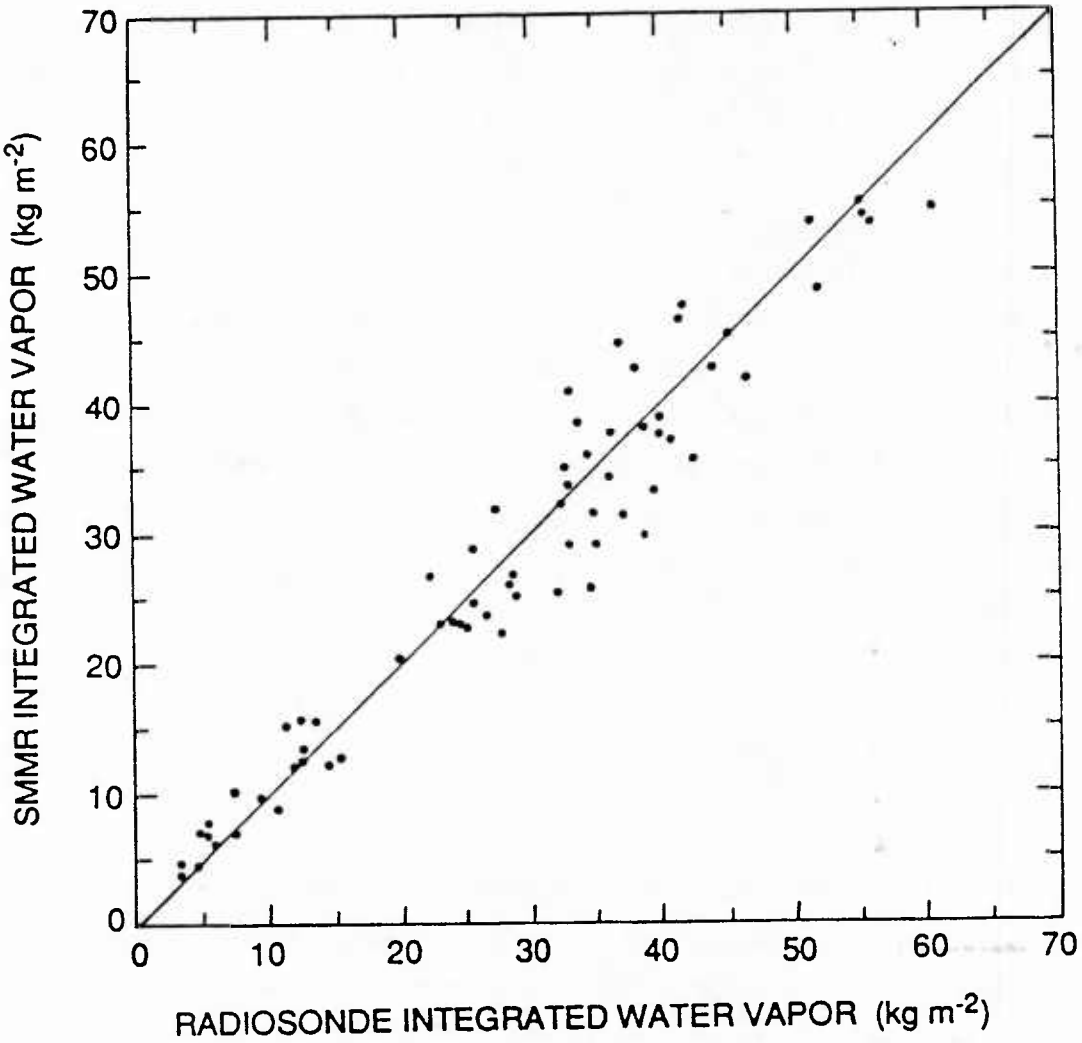

Figure 3.1 Comparison between integrated water vapor amount obtained with the Nimbus 7 SMMR to values obtained by integration of radiosonde data from weather ships and small islands.

by 120 km (two times the pixel spacing). On the edge the gradient component is computed from the difference between the pixel value itself and that of the adjacent point inward from the edge, normalized by the single-step distance (approx. 60 km). After the two components of the gradient have been found, the scalar magnitude is calculated. By examining maps of the gradient, we found that flagging values > 3.5 kg m^{-2}/60 km consistently marked the fronts in all seasons and in all areas of the global oceans without a need for scaling the parameter.

3.3 The Rain Algorithm

At present we do not feel that existing rain rate algorithms rest on a very firm foundation. The algorithm of Wilheit and Chang (1980) was certainly an appropriate approach at the time, especially since in situ data for verification are almost nonexistent over the oceans. For the less demanding purpose of locating rain areas, we have simply used a linearized version of their model results for rain rates < 5 mm/hr. Our algorithm calculates a rain rate RR (mm hr^{-1}) from:

$$RR = \frac{\left(TB_{37H} - 190\right)}{10} \qquad (3.2)$$

where TB_{37H} is the brightness temperature at 37 GHz for horizontal polarization. Since we do not want to give too much emphasis to the magnitude of the rain rate obtained from equation 3.2, especially since we believe that the threshold value 190°K must vary with surface temperature, wind speed and cloud water content, we have chosen to follow a procedure similar to the one for water vapor gradient. We simply produce a rain flag (R) where the algorithm (equation 3.2) produces a rain rate value > 0.01 mm/hr.

3.4 Case Selection

For the water vapor gradient flag and the rain indicator to be useful in diagnosing frontal locations, they must be reliable and universally applicable. We therefore tested them on mid-latitude cyclones at various stages of their life cycle, from developing wave (DW) to mature (M) and occluded (OC) stage,

and in most seasons and regions of the world ocean where these storms can be found. Some of the cases incorporated here have been the subject of more detailed analysis by our group (see previous references) and some are cases that have been published previously (e.g., Gyakum, 1983; Reed and Albright, 1986; Sanders, 1986).

3.5 Plotting Procedures and Comparison Data

Each case is plotted on three different maps; the first one shows the contours of integrated water vapor, the second shows the water vapor gradient flags (WVG-flags) of front location, and the third shows the rain-rate pattern. The surface fronts corresponding to each pass have been superimposed by using the analysis of the National Meteorological Center's map or other sources such as the Australian Weather Service Analysis, or in one case, the Berlin Weather Map, and comparing them to satellite imagery (obtained as an individual print from the NOAA, National Environmental Satellite Data and Information Service or in the document Environmental Satellite Imagery, 1979-1983). The surface frontal location has been interpolated to the time of the SMMR overpass.

The storms described by Sanders are a selection of rapidly deepening cyclones just off the east coast of the U.S. The Reed and Albright case is a rapidly deepening cyclone in the eastern North Pacific ocean. We have also studied the infamous QEII storm (Gyakum, 1983; McMurdie, et al., 1987) which damaged the ocean liner Queen Elizabeth II. We included several of these storms, since they are a serious hazard to ships at sea and, furthermore, are typically not predictable with conventional forecast methods. Real time warnings with the vapor gradient flag could possibly be a help, if we were to find that this measure is reliable. The twelve-hour interval between the sampling by SSM/I swaths at mid-latitudes may still be too infrequent to provide a sufficient warning system, since these storms often develop from a modest looking wave with an amorphous cloud system, to an exceptionally deep cyclone in less than 24 hours. In addition to the swaths listed in Appendix B we also examined 18 swaths with no frontal zones to test the null-condition, namely whether fronts would be flagged where none were present.

4. RESULTS

In this section we demonstrate that the leading edge of a strong gradient in integrated water vapor flagged by our method is co-located with the surface cold front whose position is found by traditional criterion, including satellite visible or infrared imagery. The cases studied are listed in Appendix B by region and other selection criteria, such as that they occurred during the Storm Transfer and Response Experiment (STREX) (Fleagle et al., 1982), were part of Sanders' (1986) selection of rapidly deepening cyclones or occurred during the First GARP Global Experiment (FGGE), where GARP stands for Global Atmospheric Research Program. Since the limited swath width of the SMMR's doesn't always provide the ideal sampling, we have included a sketch of the sampling and a commentary for each case, in addition to the information on whether or not the water vapor gradient flag or the precipitation measure identified the frontal zones.

4.1 Reliability of the Water Vapor Gradient Flag for Identifying Fronts

First, to show that our hypothesis was valid, we present two typical examples, one from each hemisphere, Figures 4.1 and 4.2. They show that cold fronts lie at the leading edge of strong gradients in integrated atmospheric water vapor. These two cases are not exceptionally simple and clear examples, but are representative of the great majority of the cases we have examined. None of the 18 swaths with no cyclones showed any WVG-flags. We turn now to a complex case, where the WVG-flag proves its practical value.

In Figure 4.3 we present a case where it appears that the NMC analysis failed to properly locate the surface front but the WVG-flag indicates the proper location. Figure 4.3a shows the water vapor contour map with a cold front and a conspicuous trough in the eastern half of the SMMR swath superimposed. Locations of front and trough are taken from the NMC analysis (Figure 4.3e). The WVG-flag marks the trough region (Figure 4.3b). Seeking a third opinion we obtained a European weather map for this date, the "Berliner Wetterkarte" (Figure 4.3d). This analysis shows a surface cold front in the exact location of the WVG-flags. We have used this frontal analysis to mark the surface front on Figures 4.3b and 4.3c. The infrared/visible satellite picture from GOES East also has a typical frontal cloud band in this location (Figure 4.3f). It thus

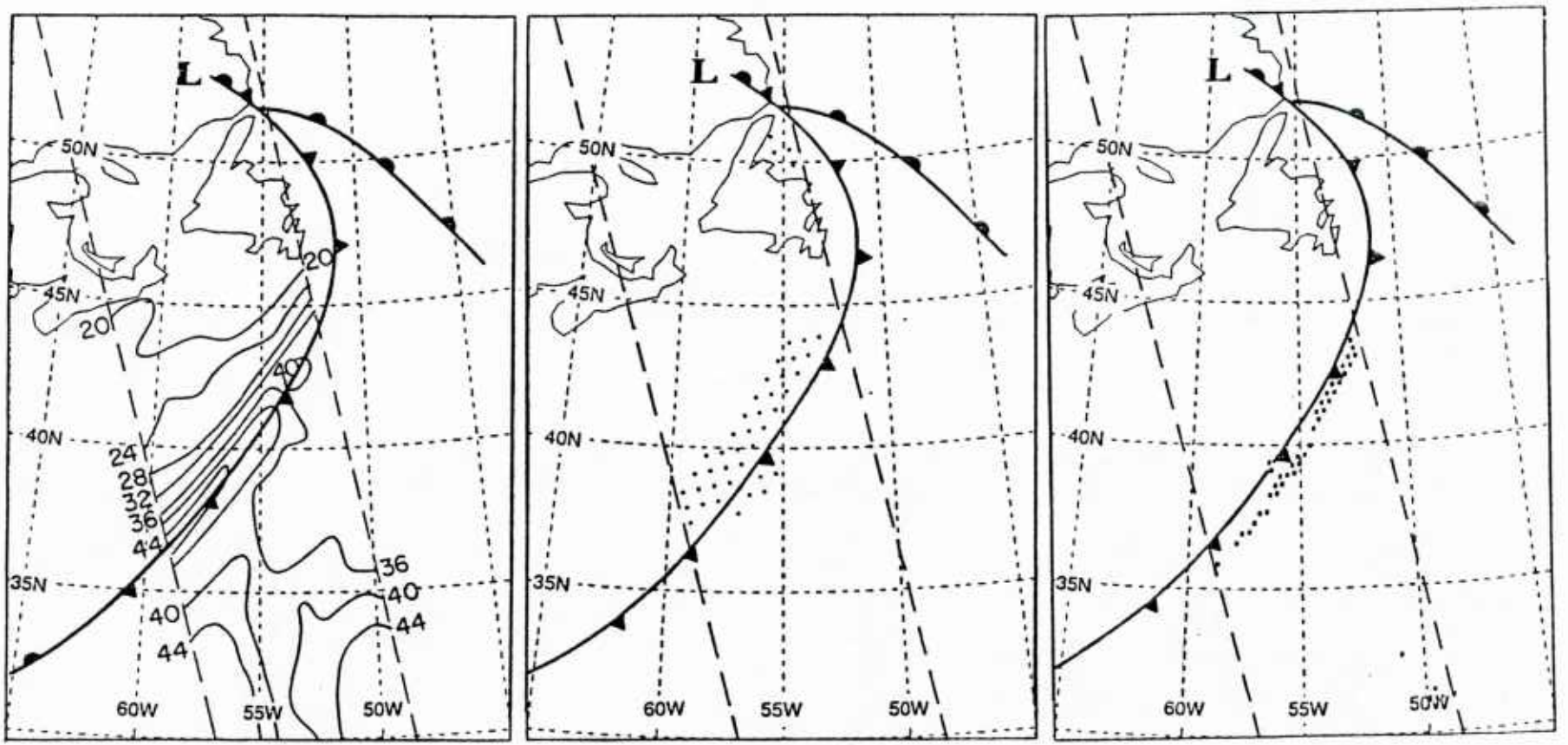

(a) Integrated water vapor in kg m^{-2}

(b) Water vapor gradient flag '*' plotted for values > 3.5 kg m^{-2}/60 km

(c) Rain occurrence

Figure 4.1 Northern hemisphere cyclone, typical case, Nimbus 7 SMMR, September 20, 1981 at 15:00 GMT, Orbit #14682, (Sanders, 1986, cases). Case #59 in Appendix B.

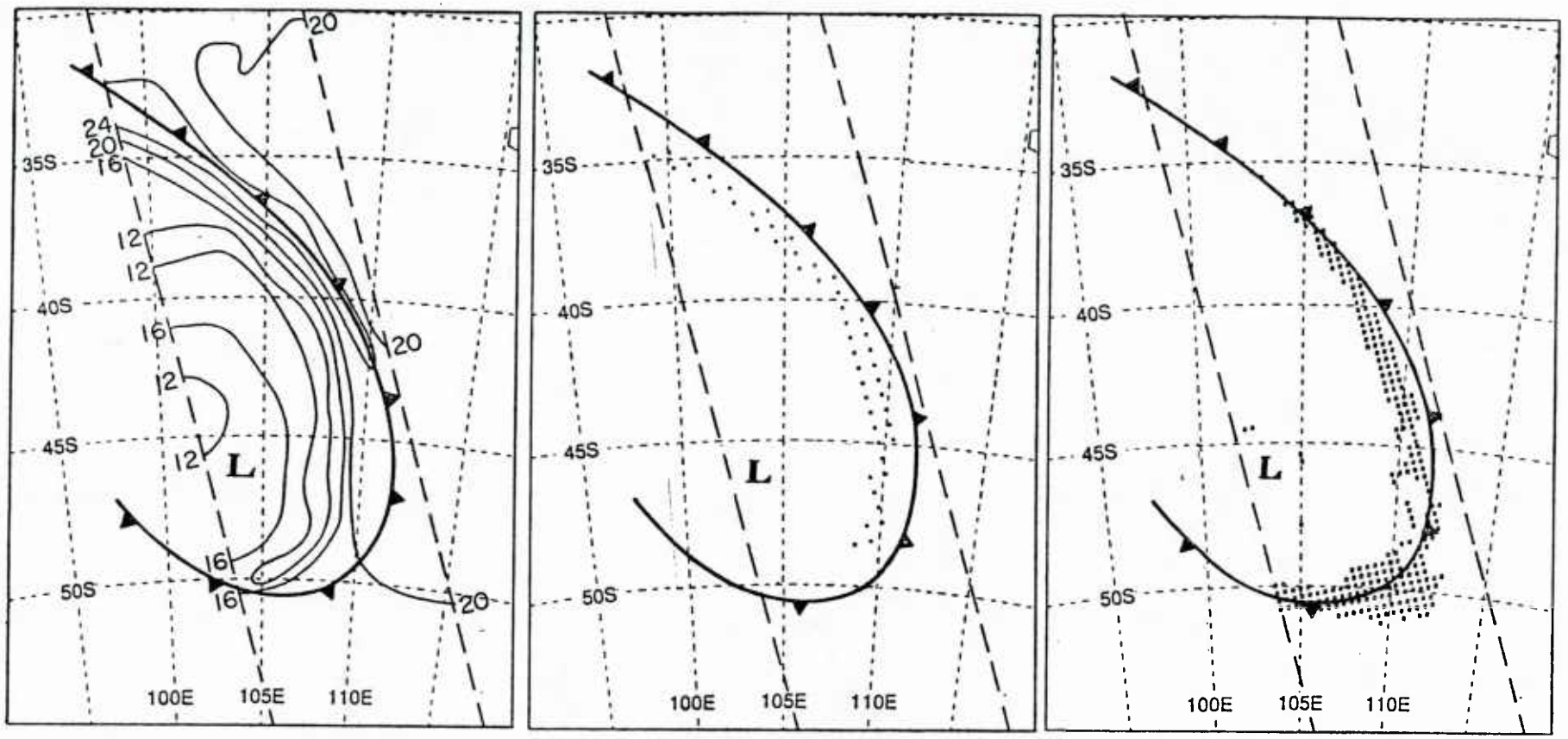

(a) Integrated water vapor in kg m^{-2}

(b) Water vapor gradient flag '*' plotted for values > 3.5 kg m^{-2}/60 km

(c) Rain occurrence

Figure 4.2 Southern hemisphere cyclone, typical case, Nimbus 7 SMMR, January 14, 1979 at 05:19 GMT, Orbit #1133, Case #23 in Appendix B.

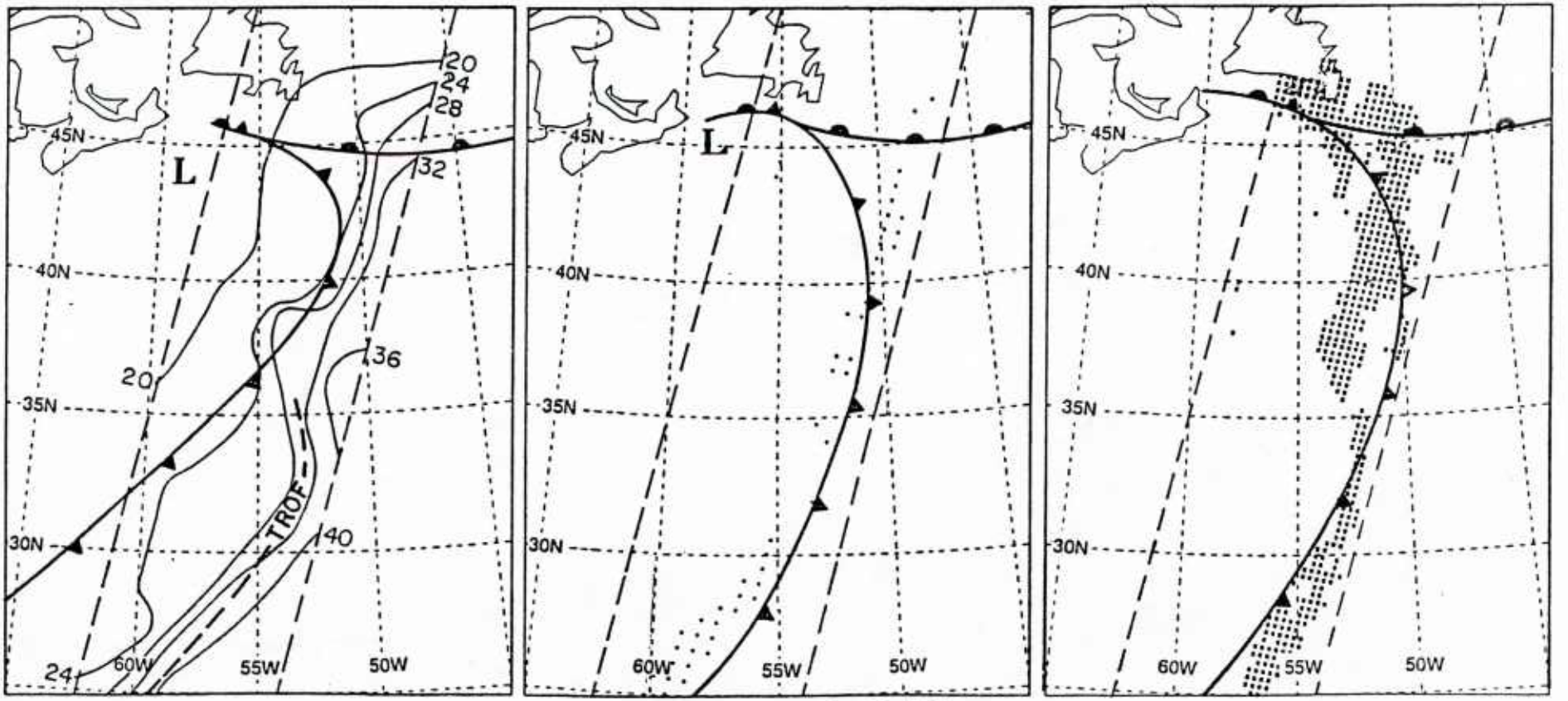

Figure 4.3 Case illustrating value of information provided by SMMR. Nimbus 7 SMMR, January 3, 1981 at 03:54 GMT, Orbit #11082. Case #50 in Appendix B. In a) the superimposed frontal and "trof" positions have been obtained from the NMC analysis at 00:00 and 06:00 GMT, while in b) the frontal position has been positioned from the "Berliner Wetterkarte" found in d), together with the NMC analysis e) (next page); f) shows the GOES East infrared image for 04:00 GMT.

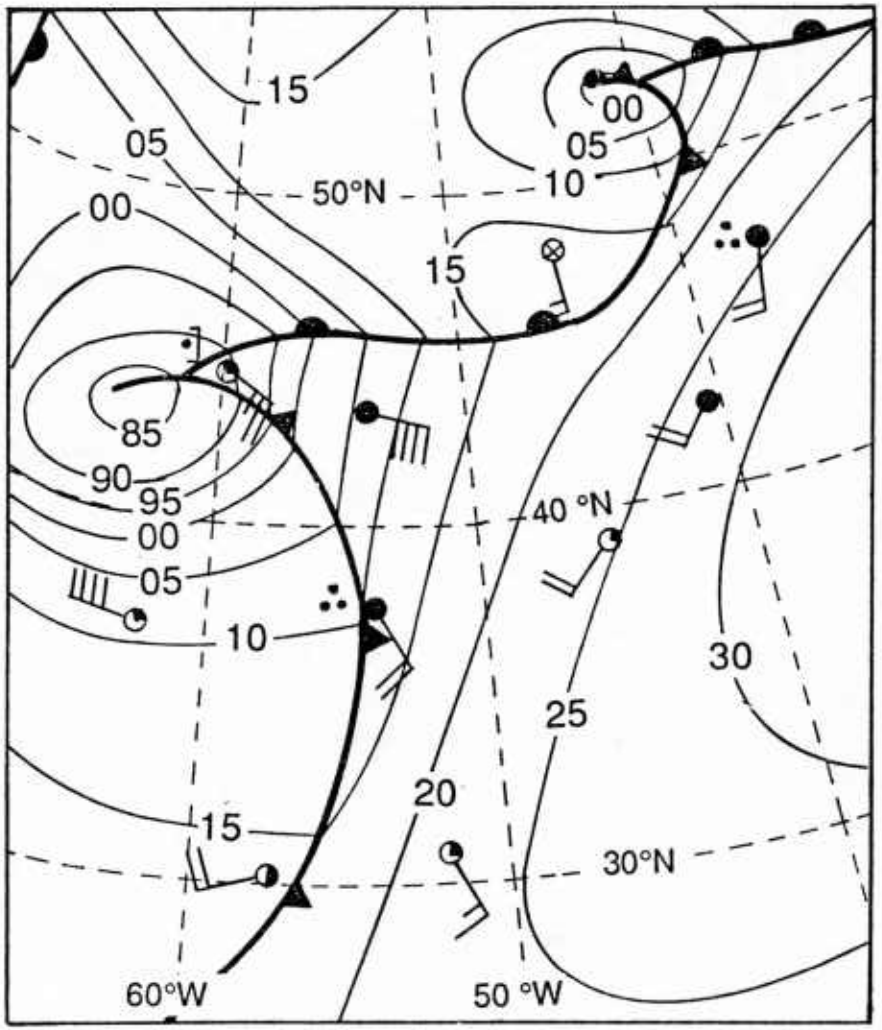

Figure 4.3d Berliner Analysis for January 3, 1981 at 00:00 GMT.

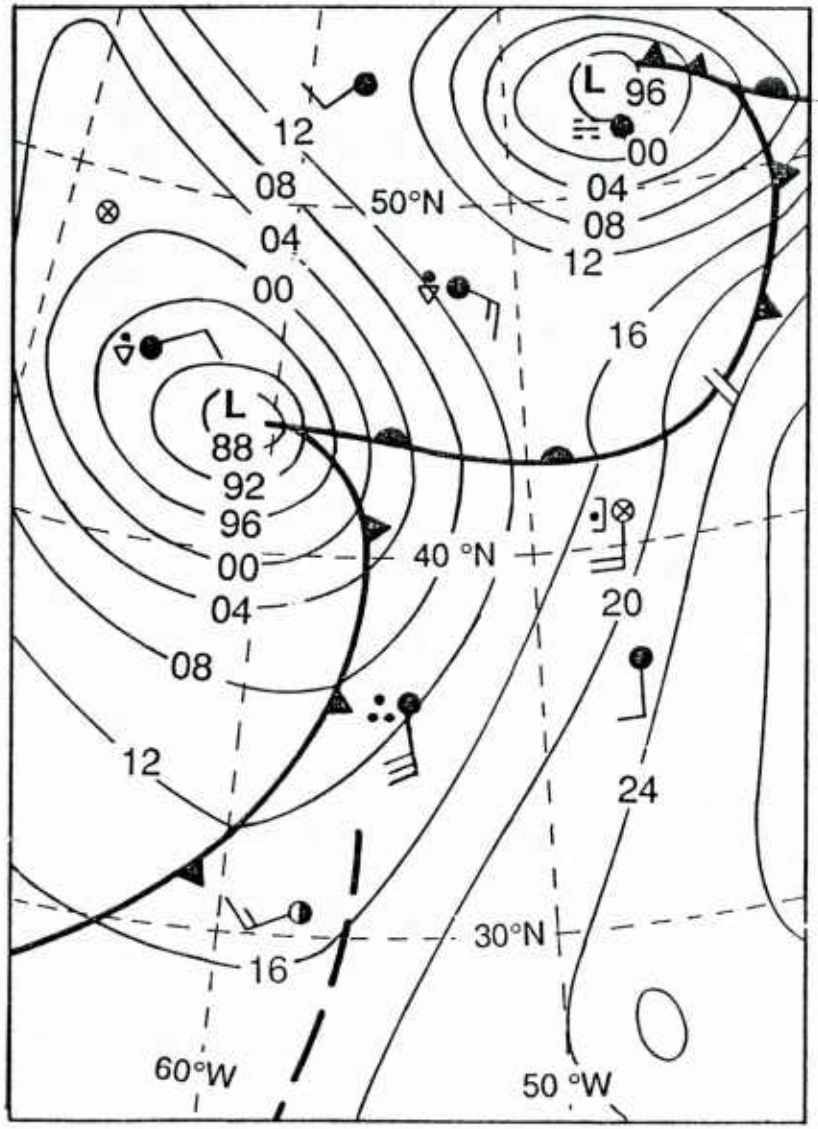

Figure 4.3e National Meteorological Center's analysis for January 3, 1981 at 00:00 GMT.

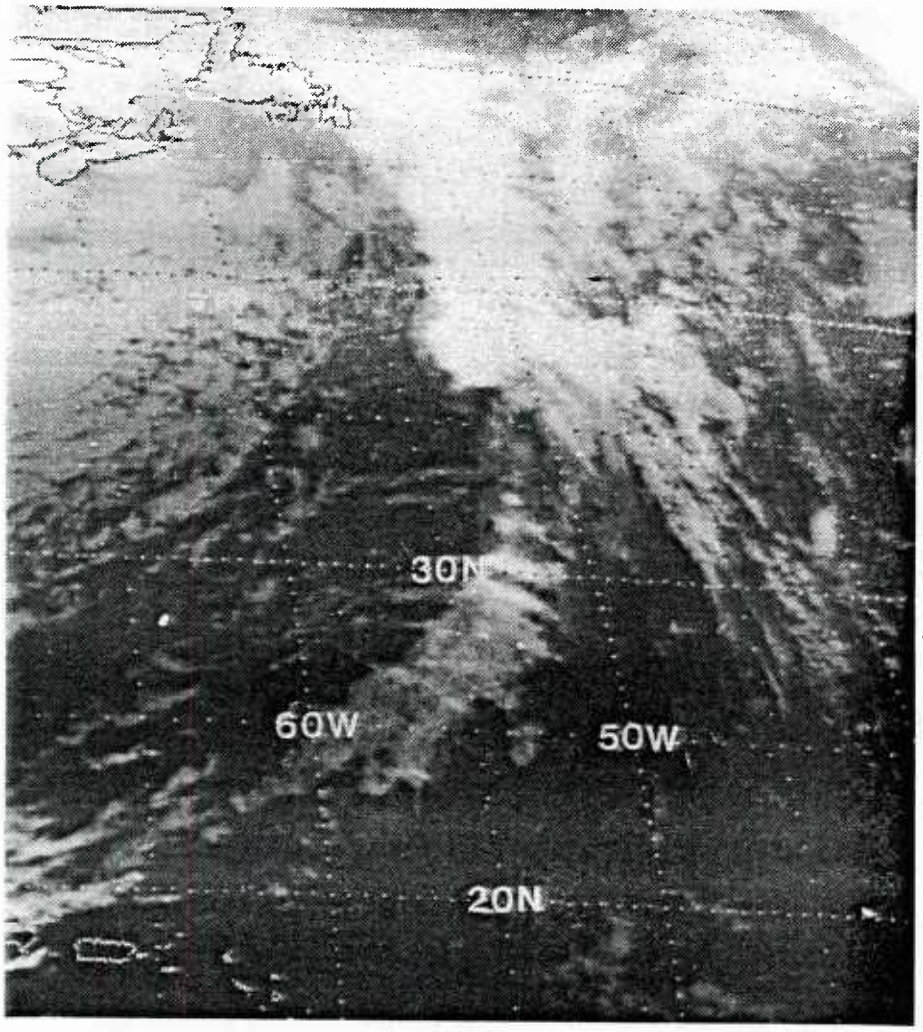

Figure 4.3f GOES West image for January 3, 1981 at 04:00 GMT.

appears that the SMMR WVG-flag could have been a useful aid to the analyst in this case.

As seen in Appendix B, SMMR's WVG-flag captures most of the warm fronts as well as the cold fronts and occluded fronts. Warm fronts are typically much less well defined than cold fronts, especially over oceanic regions. However, among the 10 definite warm fronts sampled by our study, the WVG-flag identified 9. By definite we mean those warm fronts which were clearly depicted in the Weather Service's analysis. A summary of the ability of the WVG-flag to locate fronts is found in Table 4.1, where the systems have been categorized into developing wave, mature, occluded, stationary and old ones. When the summary statistics are calculated without consideration of what type of front was sampled, the WVG-flag correctly marks 87% of all fronts.

4.2 Strong Water Vapor Gradients Flagged away from Frontal Zones

It is important for the practical use of these diagnostics to know how often one might encounter a false alarm. In the 65 swaths examined we found 6 cases where there were strong water vapor gradients, but not exactly at the location of the front. In five of these cases the extra flags occur on the warm side of the maximum in water vapor associated with the front, so that in these cases there are two lines of flags. Such lines of flags would, of course, alert an analyst. A simple example of this situation is seen in Figure 4.4, where the two bands of WVG-flags are parallel. In this case the analyst would locate the surface front between the two bands in Figure 4.4b. In Figure 4.4c this location is corroborated by the rain flag. The maximum for water vapor content has become narrow and the gradients are sharp on both sides because this is a tail end of a cold front. In cases like this one, it may be helpful if the flags were different for gradient vectors with a southward component. In case #38 over the Kuroshio current (not shown) we also observed two parallel bands of WVG-flags. The maximum in water vapor is very broad with sharp gradients around it. In this storm, there were large water vapor amounts (maximum observed 48 kg m^{-2}) and therefore the surrounding air is relatively dry, even towards the south. We suspect that the pattern is due to rain contamination of the region of the maximum water vapor content. This problem can be expected in very active systems, which often occur over warm ocean currents.

Table 4.1 Summary of efficiency of water vapor gradient flag and rain occurrence in marking frontal zones. The percentage of frontal zones flagged by the WVG is 87% and by the rain flag 91% for the 67 cases studied. See text for discussion of the relationship of these flags to frontal systems.

	Water Vapor Gradient Flag		Rain Occurrence Flag	
	Yes	No	Yes	No
Developing Wave	15	4	16	4
Mature	28	4	31	1
Occluded	13	1	12	1
Stationary	1	0	1	0
Old	1	0	1	0
Sum	58	9	61	6

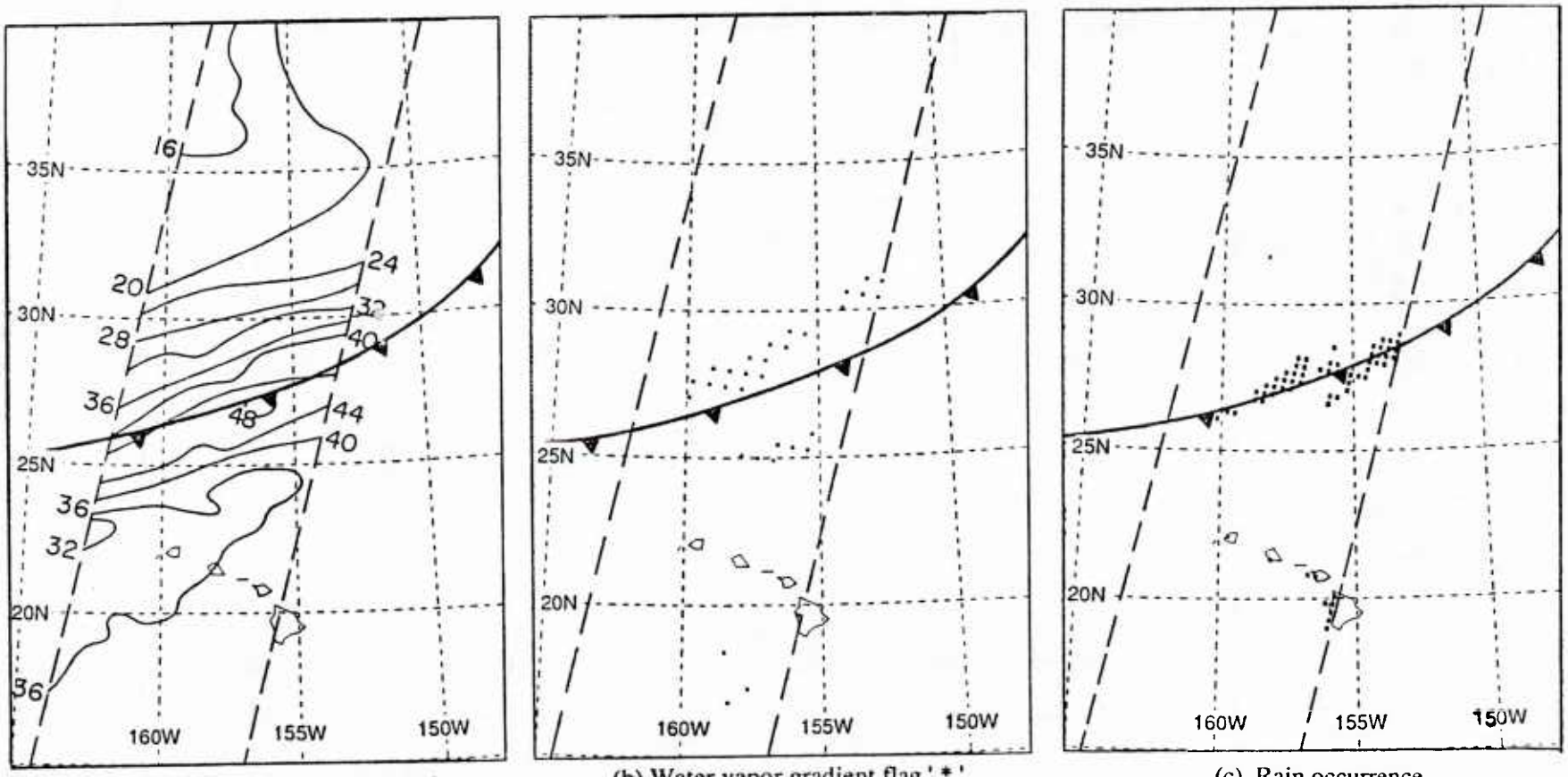

(a) Integrated water vapor in kg m^{-2}

(b) Water vapor gradient flag '*' plotted for values > 3.5 kg m^{-2}/60 km

(c) Rain occurrence

Figure 4.4 An example of a double line of WVG-flags in the vicinity of a cold front. Nimbus 7 SMMR, November 2, 1980 at 10:34 GMT, Orbit #10229. Case #1 in Appendix B.

A more complicated situation is illustrated in Figure 4.5. In addition to a mature frontal system, an old cold front exists in the region of maximum water vapor. The two extra flagged bands to the south of these fronts are simply regions of exceptionally strong gradient towards the warm dry side of the system. The old front is missed altogether by the WVG-flag. This miss does not mean that the NMC analysis was wrong, but rather that the western, more rigorous system has overtaken the cold, drier air behind the older system, thus reducing the gradient of water vapor. The satellite image (Figure 4.5d), however, does show that a cloud band is associated with the older system, so the NMC frontal analysis appears correct (Figure 4.5e).

4.3 The Rain Measure as a Locator of Fronts

Quantitative interpretation of SMMR brightness temperatures in terms of rain rate is complicated by the dependence of the brightness temperatures on other unmeasured quantities. Examples are fractional footprint filling by rain, rain layer depth, coexistence of rain with highly variable amounts of nonprecipitating cloud water, surface roughness, etc. However, as a detector of precipitation of some areal extent and intensity it appears that even a simple algorithm such as equation 3.2 is adequate. Most of the frontal zones captured with the WVG-flag also showed regions where the precipitation measure was greater than the threshold value (but the two measures were not necessarily overlapping as can be seen by comparing subfigures b and c of Figures 4.1, 4.2 and 4.3). The strong water vapor gradients away from the main low pressure center generally did not show large scale precipitation. Thus, the combination of the two measures is stronger than the WVG-flag technique alone.

5. DISCUSSION AND RECOMMENDATIONS

Our analysis of 67 fronts in most parts of the global ocean and in most seasons shows that the water vapor gradient pattern is closely related to surface fronts, particularly cold fronts and occluded fronts. It is remarkable that the flag based on a constant threshold value of this gradient, of > 3.5 kg $m^{-2}/60$ km was 87% correct in outlining such frontal zones regardless of season or region in question. Thus, this flag could be a quick and reliable measure for locating surface fronts. It does not necessarily provide information on frontal location which is better than what is already available to a trained eye from visible or

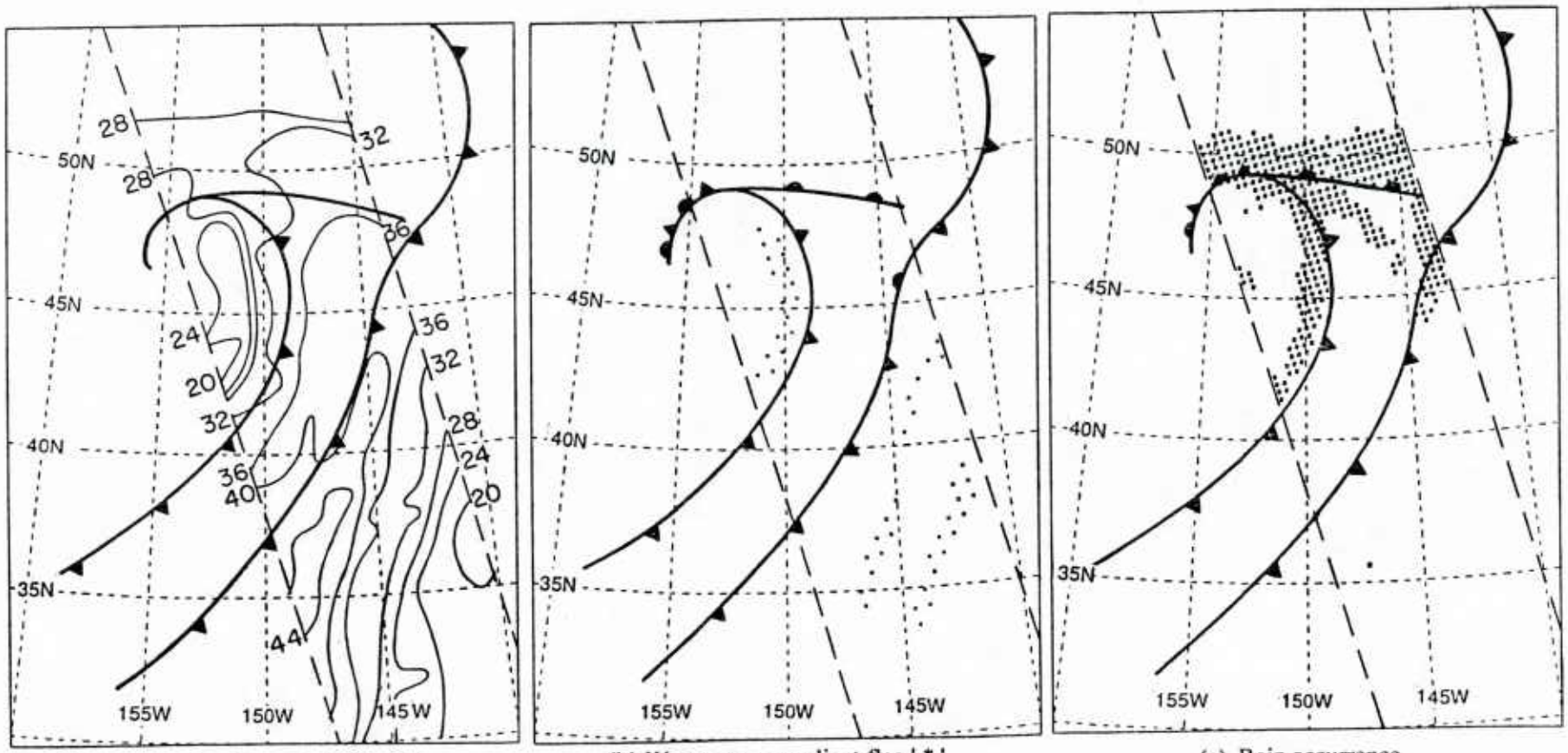

(a) Integrated water vapor in kg m^{-2}

(b) Water vapor gradient flag '*' plotted for values > 3.5 kg m^{-2}/60 km

(c) Rain occurrence

Figure 4.5 This is a representative problem case from the North Pacific, Nimbus 7 SMMR, September 11, 1979 at 20:58 GMT, Orbit #4459. Case #40 in Appendix B. There are two frontal zones in close proximity, according to the NMC analysis. Only one is indicated by the WVG- and R-flag in b) and c). In b) we also see two zones to the south indicated by the WVG-flag. The GOES West infrared image, and the weather map for 18:00 GMT are found in Figures 4.5 d) and e) (next page). Obviously, the flagged zones in b) correspond to the spiral cloud bands in this occluded old cyclone.

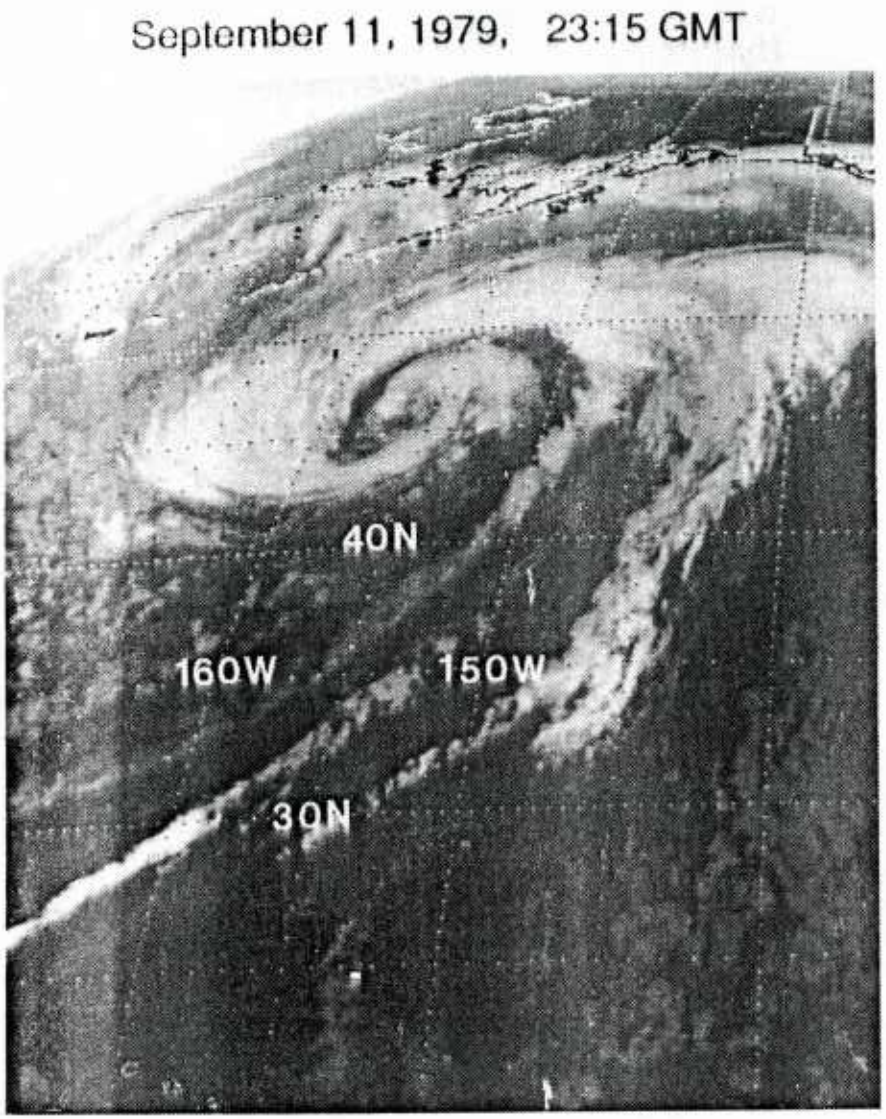

Figure 4.5d The GOES West image

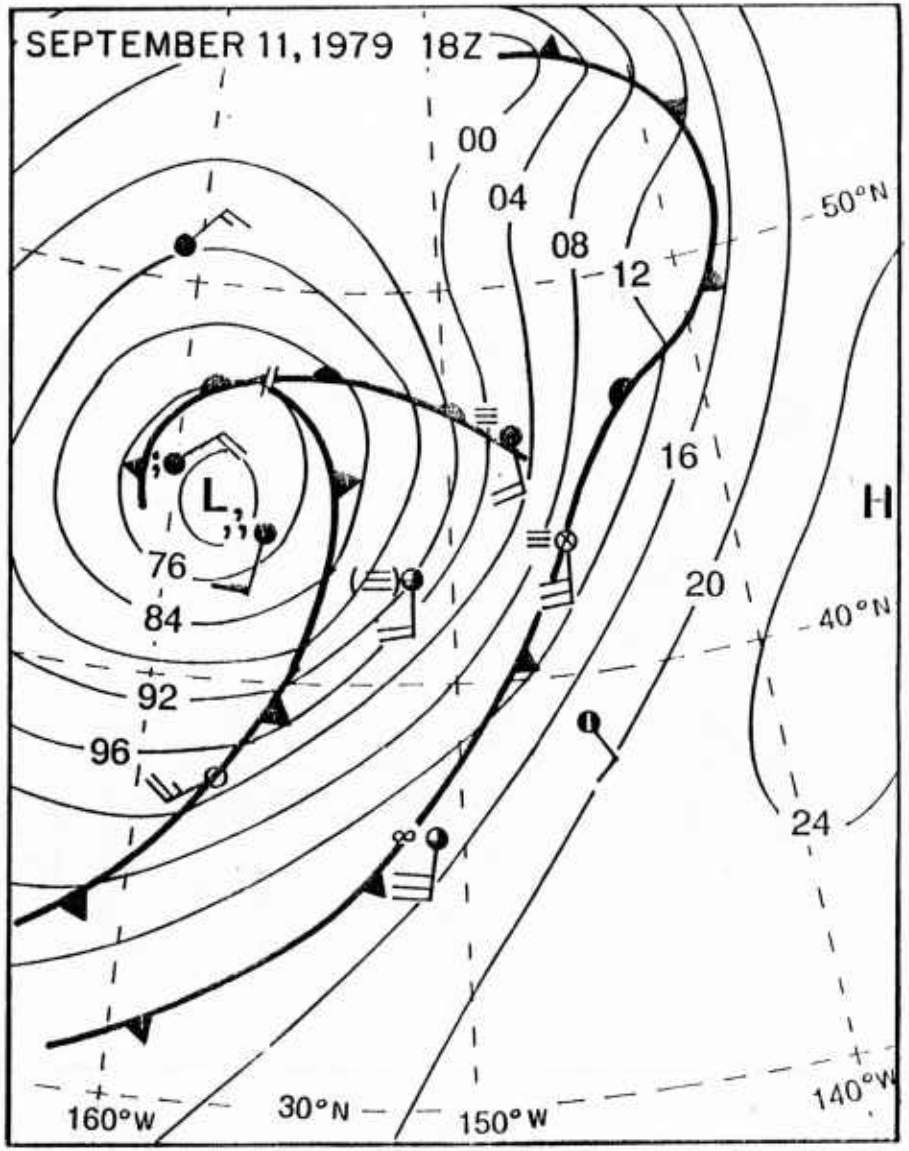

Figure 4.5e The weather map

infrared satellite imagery. However, in this form it is less dependent on the analyst's judgment and may have an advantage when a cirrus shield is exceptionally dense or diffuse. Combining the WVG-flag with the precipitation locator, one can be even more certain that a frontal zone has been located.

The rain flag captures the activity near the apex between warm and cold fronts and often shows rain ahead of the warm front, while the WVG-flag is more closely related to the cold or warm front away from the low center. The rain flag is not as closely tied to the frontal zones, but often marks a wide area surrounding the frontal zones. It is, therefore, not as simple to interpret as the WVG-flag but from the present evidence appears slightly more dependable as a flag for cyclonic activity.

The information content of the contour maps of integrated atmospheric water vapor is, of course, much greater than the maps with the WVG-flag alone. However, interpreting the contour maps requires a deeper understanding by the analyst on duty, which consequently requires more training. It would take more time and effort to interpret such a picture, and more computer software and hardware to produce the contour maps. However, this difference is minor. Thus, we would recommend that the contour maps of water vapor be available to call up by the analyst, but that the flagging routine be the "first look" tool.

We recommend that these diagnostic tools now be applied to SSM/I data as soon as they become available. We expect to carry out this work ourselves, but would welcome collaboration, particularly with active forecasters.

Because the water vapor channel on SSM/I employs a frequency closer to the center of the 22 GHz emission line, the signals will be stronger. The threshold value for flagging fronts should not be different since it is based on the value of the integrated water vapor gradient which should be independent of the sensor. However, since SSM/I will provide somewhat greater areal resolution it may allow a more fine-tuned threshold.

In order to avoid flagging strong gradients on the equatorward side of water vapor maxima, one could develop a criterion based on the gradient vector rather than the scalar magnitude. However, since frontal zones can take on a wide range of orientations, this may require an increase in complexity of the algorithm, which is likely to cause "failures" as often as the present extremely simple method. Providing WVG- and R-flags in combination is probably the most profitable approach.

* * *

Acknowledgments

We are grateful to Drs. Daesoo Han, Per Gloersen and Paul H. Hwang (NASA/Goddard Space Flight Center), members of the SMMR Nimbus experiment and Information Processing Teams, and the National Space Science Data Center for providing us the Cell-All data tapes used for this study. We also appreciate the encouragement of Drs. Andreas Goroch and Paul Tag at the Naval Environmental Prediction Research Facility. We thank Ms. Janet Meadows who typed the report.

REFERENCES

Alishouse, J.C., 1983: Total Precipitable Water and Rainfall Determinations from the Seasat Scanning Multichannel Microwave Radiometer (SMMR). J. Geophys. Res., 88, 1929-1935.

Anderson, R.K., J.P. Ashman, F. Bittner, G.R. Farr, E.W. Ferguson, V.J. Oliver and A.H. Smith, 1969: Applications of Meteorological Satellite Data in Analysis and Forecasting. ESSA Tech. Rep. NESC 51, (available from Govt. Printing Office, Washington, D.C.), pp. 38.

Bjerknes, J., 1919: On the Structure of Moving Cyclones. Geofysics Publ. 1, 1-8.

Bjerknes, J. and H. Solberg, 1922: Life Cycle of Cyclones and the Polar Front Theory of Atmospheric Circulation. Geofys. Publ. 3., 3-18.

Chang, H.D., P.H. Hwang, T.T. Wilheit, A.T.C. Chang, D.H. Staelin and P.W. Rosenkranz, 1984: Monthly Distributions of Precipitable Water from the Nimbus 7 SMMR Data. J. Geophys. Res., 89, 5328-5334.

Chang, A.T.C. and T.T. Wilheit, 1980: Remote Sensing of Water Vapor, Liquid Water, and Wind Speed at the Ocean Surface by Passive Microwave Techniques from the Nimbus-5 Satellite. Radio Science, 14, 793-802.

Environmental Satellite Imagery, 1979-1983: Key to Meteorological Records Documentation. NOAA, Environmental Data and Information Service, National Environmental Satellite Service, Washington, D.C., (one volume per month), pp. 66.

Fleagle, R.G., M. Miyake, J.F. Garrett and G.A. McBean, 1982: Storm Transfer and Response Experiment. Bull. Am. Meteorol. Soc., 63, 6-14.

Gloersen, P. and F.T. Barath, 1977: A Scanning Multichannel Microwave Radiometer for Nimbus-G and Seasat-A. IEEE J. Ocean. Eng., OE2, 172-178.

Gloersen, P.D, D.J. Cavalieri, A.T.C. Chang, T.T. Wilheit, W.J. Campbell, O.M. Johannessen, K.B. Katsaros, K.F. Kunzi, D.B. Ross, D. Staelin, E.P.L. Windsor, F.T. Barath, P. Gudmandsen, E. Langham and R.O. Ramseier, 1984: A Summary of Results from the First Nimbus 7 SMMR Observations. J. Geophys. Res., 89, 5335-5344.

Gyakum, J.R., 1983: On the Evolution of the QEII storm. I: Synoptic aspects. Mon. Wea. Rev., 111, 1137-1155.

Katsaros, K.B., I.A. Bhatti, L.A. McMurdie and G.W. Petty, 1987: Passive Microwave Data used for Diagnosis of Fronts in Cyclonic Storms. Interim Technical Report Number 1 on Contract N0014-86-K-0453, pp. 21, Dept. of Atmospheric Sciences, AK-40, University of Washington, Seattle, WA 98195, (available from the authors), pp. 21.

Katsaros, K.B. and R.M. Lewis, 1986: Mesoscale and Synoptic Scale Features of North Pacific Weather Systems Observed with the Scanning Multichannel Microwave Radiometer on Nimbus 7. J. Geophys. Res., 91, 2321-2330.

Katsaros, K.B., P.K. Taylor, J.C. Alishouse and R.J. Lipes, 1981: Quality of Seasat Scanning Multichannel Microwave Radiometer (SMMR) Atmospheric Water Determinations. In Oceanography From Space, edited by J.F.R. Gower, pp. 691-706, Plenum, New York.

Kim, S.T., D. Han and H.D. Chang, 1985: Analysis and Correction of the Brightness Temperature Measured in the 21GHz Horizontal Channel of the Nimbus-7 Scanning Multichannel Microwave Radiometer. Systems and Applied Sciences Corp., 5809 Annapolis Road, Hyattsville, MD 20784, Document No. SASC-T-5-5100-0004-0026-84, (available from the authors), pp. 51.

McMurdie, L.A. and K.B. Katsaros, 1985: Atmospheric Water Distribution in a Mid-latitude Cyclone observed by the Seasat Scanning Multichannel Microwave Radiometer. Mon. Wea. Rev., 113, 584-598.

McMurdie, L.A., G. Levy and K. B. Katsaros, 1987: On the Relationship between Scatterometer Derived Convergences and Atmospheric Moisture. Mon. Wea. Rev., 115, 1281-1294.

Njoku, E.G., E.J. Christensen and R.E. Cofield, 1980: The Seasat Scanning Multichannel Microwave Radiometer Antenna Pattern Correction Development and Implementation. IEEE J. Ocean. Eng., 125-137.

Prabhakara, C., H.D. Chang and A.T.C. Chang, 1982: Remote Sensing of Precipitable Water over the Oceans from Nimbus 7 Microwave Measurements. J. Appl. Meteor., 21, 59-68.

Reed, R.J. and M.D. Albright, 1986: A Case Study of Explosive Cyclogenesis in the Eastern Pacific. Mon. Wea. Rev., 114, 2297-2319.

Rosenkranz, P.W., D.H. Staelin and N.C. Grody, 1978: Typhoon June (1975) Viewed by Scanning Microwave Spectrometer. J. Geophys. Res., 83(C4), 1857-1868.

Sanders, F.W., 1986: Explosive Cyclogenesis in the West-Central North Atlantic Ocean, 1981-84. Part I: Composite Structure and Mean Behavior. Mon. Wea. Rev., 114, 1781-1794.

Seasat Geophysical Data Record User's Guide, Scanning Multichannel Microwave Radiometer (SMMR). Document 622-205, Rev. A, NASA, Jet Propulsion Laboratory, California Institute of Technology, August 1982, (available from JPL), pp. 88.

SMMR Mini-Workshop IV, Report. Document 622-234, NASA, Jet Propulsion Laboratory, California Institute of Technology, 1 December 1981, (available from JPL), pp. 138.

Staelin, D.H., K.F. Kunzi, R.L. Pettyjohn, R.K.L. Poon, R.W. Wilcox and J.W. Waters, 1976: Remote Sensing of Atmospheric Water Vapor and Liquid Water with the Nimbus-5 Microwave Spectrometer. J. Appl. Meteorol., 15, 1204-1214.

User's Guide for the Nimbus-7 Scanning Multichannel Microwave Radiometer (SMMR) PARM and MAP Tapes, 1983. Systems and Applied Sciences Corporation, 5809 Annapolis Road, Hyattsville, MD 20784, pp. 68.

Wilheit, T.T. and A.T.C. Chang, 1980: An Algorithm for Retrieval of Ocean Surface and Atmospheric Parameters from the Observations of the Scanning Multichannel Microwave Radiometer (SMMR). Radio Science, 15, 525-544.

APPENDIX A

ALGORITHM USED FOR CALCULATING INTEGRATED WATER VAPOR AND THE WATER VAPOR GRADIENT

A1.1 The Staelin-Rosenkranz Water Vapor Algorithm

The algorithm for integrated Water Vapor (WV) uses the 18, 21 and 37 GHz SMMR channels in both polarizations as follows:

$$W = 2.0 + 0.1V + 0.0011V^2 \quad \text{(cm)} \tag{A1.1}$$

where

$$\begin{aligned} V = {} & -0.405\,(T_{18H} - 105.5) - 0.165\,(T_{18V} - 173.3) \\ & +0.489\,(T_{21H} - 139.8) + 0.382\,(T_{21V} - 195.7) \\ & -0.225\,(T_{37H} - 141.0) + 0.250\,(T_{37V} - 204.0) \end{aligned} \tag{A1.2}$$

This algorithm was fine-tuned by comparing radiosonde observations from ships with coincident SMMR data for the period February 15-27, 1979. After tuning, the retrieved water vapor is

$$W' = 1.085\,W - .228 \quad \text{(cm)} \tag{A1.3}$$

We have converted this measure of water vapor (precipitable cm's) to S.I. units: 1 cm corresponds to 10 kg m-2. The standard deviation of the water vapor retrieval is 0.21 cm (Chang, et al., 1984).

A1.2 The Algorithm for Calculating the Water Vapor Gradient

Let W_{ij} = (i, j)th value of the 13 x 13 block of retrieved water vapor values (kg m^{-2}) (i, j = 1, 2, ..., 13)

Let Gx_{ij} = x-component of the gradient of W calculated at element i, j.

and Gy_{ij} = y-component of the gradient of W calculated at element i, j.

$$\text{Then } G_{x,ij} = \frac{W_{il,j} - W_{i\emptyset,j}}{il - i\emptyset}$$

where il = minimum of {i+1, 13}
$i\emptyset$ = maximum of {i-1, 1}

$$\text{Likewise } G_{y,ij} = \frac{W_{i,jl} - W_{i,j\emptyset}}{jl - j\emptyset}$$

where jl = minimum of {j+1, 13}
$j\emptyset$ = maximum of {j-1, 1}

The scalar magnitude of the gradient of W is just:

$$\gamma_{ij} = \left| \left(G_{x,ij}, G_{y,ij} \right) \right| = \sqrt{G^2_{x,ij} + G^2_{y,ij}}.$$

Units of γ_{ij} are (kg m^{-2}) per pixel spacing
$\simeq$ (kg m^{-2}) per 60 km for Nimbus 7 SMMR.

APPENDIX B

CYCLONIC STORMS STUDIED WITH SMMR DATA

No	Date	Time GMT	Rev. #	Center of Swath Lat/Lon	Max. Vapor Kg/m²	Min. Vapor Kg/m²	WV Flag Catches	Rain Signal Catches
STREX CASES (Storm Transfer & Response Experiment)								
1	11/2/80	10:34	10229	35N/155W	44	20	Yes CF	Yes CF
2	11/6/80	10:06	10284	37N/147W	44	16	Yes CF	Yes L
3	11/14/80	10:52	10395	42N/157W	36	12	Yes CF	Yes CF + L
4	11/16/80	11:27	10423	45N/165W	28	10	Yes CF	Yes CF + L
5	11/16/80	21:25	10429	45N/153W	24	8	Yes CF	Yes J +CF
6	11/18/80	10:19	10450	45N/150W	28	8	Yes WF	Yes WF
7	11/18/80	20:19	10456	45N/138W	28	12	No	Yes WF
8	11/18/80	21:59	10457	37N/160W	32	12	Yes CF	Yes CF
9	11/20/80	09:13	10477	42N/132W	32	8	Yes CF	Yes CF
10	11/20/80	20:56	10484	42N/145W	32	12	Yes CF	Yes CF

Key for the symbols:

CF for "Cold Front"
WF for "Warm Front"
J for "Junction of storm"
L for "Low"
DW for "Developing Wave"
OF for "Old Front"
OC for "Occluded"

No	Sketch of SMMR Swath	Qualitative Assessment
STREX CASES (Storm Transfer & Response Experiment)		
1		Flagging subroutine appears to locate the cyclone. GOOD
2		Strong gradient behind cold front; OF and CF are easily located GOOD
3		Wave development along cold front does not signal; water vapor max is far ahead of CF. OK
4		Pattern correlates very well with all the frontal locations. Strong gradient at 45N behind CF in cold air. V. GOOD
5		Same storm as 4. Pattern similar. Fronts correspond well to pattern. V. GOOD
6		NMC WF orientation does not align with pattern. Max far south of WF (4-5 deg) OK
7	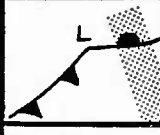	WF orientation does not align with SMMR pat. Complicated frontal analysis OK
8		Two CFs close to each other are sampled. The max and gradient are broader than normal. There is max at each front. GOOD
9		Good correlation between pattern and CF.
10		The pattern correlates reasonably well with CF. Low has no distinguishing pattern. Max gradient much broader than other cases. GOOD

Continued

APPENDIX B:

CYCLONIC STORMS STUDIED WITH SMMR DATA.

No	Date	Time GMT	Rev. #	Center of Swath Lat/Lon	Max. Vapor Kg/m²	Min. Vapor Kg/m²	WV Flag Catches	Rain Signal Catches
11	11/22/80	09:50	10505	46N/140W	20-28 28-32	12	Yes CF NO CF	Yes CF Yes CF
12	11/24/80	20:26	10539	42N/137W	34	11	Yes CF	Yes CF
13	11/24/80	22:07	10540	33N/161W	40	12	Yes WF	Yes L
14	11/26/80	09:22	10560	42N/135W	33	22	Yes WF	Yes J
15	11/28/80	10:00	10588	40N/145W	40	10	Yes CF	Yes CF
FGGE CASES -- NORTH PACIFIC								
16	1/10/79	11:54	1081	40N/175W	20	12	NO	Yes CF
17	1/10/79	21:47	1087	37N/158W	40	12	Yes CF	Yes CF
18	1/12/79	09:06	1107	34N/132W	34	8	Yes CF	Yes CF
19	1/12/79	20:42	1114	42N/143W	20 32	10 20	Yes CF NO CF	Yes CF Yes CF
20	1/14/79	09:39	1135	35N/142W	44	10	Yes CF	No

Key for the symbols:

CF for "Cold Front"
WF for "Warm Front"
J for "Junction of storm"
L for "Low"
DW for "Developing Wave"
OF for "Old Front"
OC for "Occluded"

No	Sketch of SMMR Swath	Qualitative Assessment
11		Good correlation between pattern and fronts. Pattern is inverted V with apex along the OF Typical case. V. GOOD
12		Moisture band broader than most storms at this stage. Minimum behind and ahead of CF GOOD- V. GOOD
13		Max to south of WF. Contour lines roughly align along the WF.
14		Pattern does not correspond very well with fronts. Possible analysis time too far off and only warm sector is sampled. POOR
15	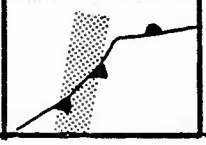	Strongest gradient behind CF location, CF lies along max. Contours imply large cloud shield north of Low. V. GOOD
FGGE CASES		(First Garp Global Experiment)
16		Pattern somewhat disorganized. No clearcut orientation of gradient. Broad correlation with FGGE gridded data. OK
17	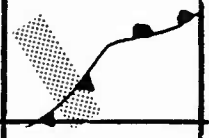	Northern system is missed. But tail of old system is clearly seen with high max and strong gradient. OK
18		Samples stationary front with a narrow band of moisture aligned with front. Gradients moderate-strong on each side of max. GOOD
19		Weak signal in vapor pattern near CF. Steady increase towards the south with 2nd max at south front OK - GOOD
20		Area near Low has weak local maximum, otherwise field is rather uniform, until tail of CF OK - GOOD

Continued

APPENDIX B:

CYCLONIC STORMS STUDIED WITH SMMR DATA.

No	Date	Time GMT	Rev.#	Center of Swath Lat/Lon	Max. Vapor Kg/m^2	Min. Vapor Kg/m^2	WV Flag Catches	Rain Signal Catches
21	1/14/79	19:33	1141	40N/125W	30	12	Yes CF	Yes J
22	1/22/79	10:15	1246	43N/147W	24	8	Yes CF + L	Yes CF + L
SOUTHERN HEMISPHERE CASES								
23	1/14/79	05:17	1133	44S/107E	27	12	Yes CF	Yes CF
24	9/ 3/79	14:11	4345	46S/135E	21	4	No	NO CF + J
25	9/ 3/79	15:53	4346	43S/110E	21	5	Yes CF	Yes CF
26	9/ 5/79	13:03	4372	47S/153E	32 19	12 7	Yes CF No L	Yes CF Yes L
NORTH ATLANTIC CASES								
27	1/18/79	1532Z	1194	35N/64W	26	7	Yes CF	Yes CF
28	01/01/83	12:03	21149	50N/16W	26	8	No CF	No CF
29	01/05/83	01:28	21198	57N/14W	24	12	Yes CF	Yes CF

Key for the symbols:

CF for "Cold Front"
WF for "Warm Front"
J for "Junction of storm"
L for "Low"
DW for "Developing Wave"
OF for "Old Front"
OC for "Occluded"

No	Sketch of SMMR Swath	Qualitative Assessment
21	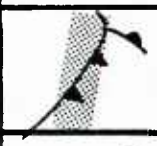	Broad field at OF and behind in cold air. A Low in local max. CF has distinct max. GOOD
22		Wave distinquished in shape of contour lines. Band of moisture narrow, with minimum to south around 32N. V. GOOD
SOUTHERN HEMISPHERE CASES		
23		Max is narrow band oriented paralled to and exactly ahead of front. Pattern highly correlated with synoptic situation. V. GOOD
24		Region of max vapor assoc. with front. Wave not obvious in vapor pattern. OK
25		Band of max vapor associated with CF. Strong gradient towards pole. GOOD
26		Max at 30S ahead of CF. Second max at Low. GOOD
NORTH ATLANTIC CASES		
27		Mins low to North. Gradient near front not oriented same as CF. Otherwise looks normal. GOOD
28		Max a little far ahead of CF. Some indication of development in vapor pattern. GOOD
29		Front appears weak with broad water vapor gradient. Poor

Continued

APPENDIX B:

CYCLONIC STORMS STUDIED WITH SMMR DATA.

No	Date	Time GMT	Rev. #	Center of Swath Lat/Lon	Max. Vapor Kg/m²	Min. Vapor Kg/m²	WV Flag Catches	Rain Signal Catches
30	01/07/83	13:52	21233	45N/40W	22	12	Yes WF	
31	02/02/83	13:11	21592	50N/33W	32	24	No CF Yes WF	Yes CF Yes WF
32	05/19/83	12:44	23057	50N/30W	30	20 30	Yes WF Yes (Trof)	Yes WF No (Trof)
33	05/21/83	01:35	23078	52N/20W	22	10	Yes WF	No WF
34	05/21/83	13:22	23085	47N/33W	28	12	Yes CF	Yes CF
35	05/27/83	13:29	23168	47N/37W	32	16	Yes CF	Yes J
KURISHIO (NORTH PACIFIC STORMS)								
36	9/7/79	09:47	4397	40N/142W	34 25	14 16	Yes CF No L	Yes CF Yes L
37	9/7/79	19:45	4403	45N/126W	34	17	Yes CF	Yes CF + L
38	9/9/79	23:49	4433	42N/173E	48	18	Yes CF + L	Yes CF + L

Key for the symbols B:

CF for "Cold Front"
WF for "Warm Front"
J for "Junction of storm"
L for "Low"
DW for "Developing Wave"
OF for "Old Front"
OC for "Occluded"

No	Sketch of SMMR Swath	Qualitative Assessment
30		Strong gradient south of main WF 30-35 N. Max. close to and ahead of the WF. Old WF tail has little correlation with vapor pattern. OK
31		Two weak frontal systems sampled. WV pattern is somewhat disorganized. Values at Low show no gradient. POOR
32		Strong gradient ahead of the trof. Max. lies at the SW of the trof. A typical case. GOOD
33		Low water vapor values but strong gradient ahead of WF. European weather map does agree with SMMR analysis. GOOD
34		A typical case with strong gradient ahead of CF. SMMR pattern fits well the hypothesis. GOOD
35		A weak occluded storm with weak gradient. Water vapor contours do orient along the system. OK
KUROSHIO (NORTH PACIFIC CASES)		
36		Max a little far ahead of CF, otherwise gradient in vicinity of CF. Near Low local max indicates clouds/rain. OK
37		Max far ahead of CF, even if CF analyzed at 20Z. Otherwise pattern is typical with band of moisture agreeing with CF. OK
38		Possible rain interference, especially near Low, otherwise, pattern looks normal with gradient behind CF. GOOD

Continued

APPENDIX B:

CYCLONIC STORMS STUDIED WITH SMMR DATA.

No	Date	Time GMT	Rev.#	Center of Swath Lat/Lon	Max. Vapor Kg/m²	Min. Vapor Kg/m²	WV Flag Catches	Rain Signal Catches
39	9/11/79	11:02	4453	43N/160W	36 42 32	16	Yes CF Yes CF Yes L	Yes CF No CF Yes L
40	9/11/79	20:58	4459	43N/147W	36	20	Yes CF	Yes CF + J
41	9/13/79	09:55	4480	43N/143W	42	19	Yes CF	Yes CF
42	09/13/79	13:26	4482	35N/165E	43	15	Yes CF + L	Yes CF + L
43	1/2/82	21:11	16123	42N/150W	32	14	No	Yes CF
44	3/7/82	10:48	17029	46N/155W	25	17	Yes CF	Yes CF
45	3/7/82	20:48	17035	47N/145W	24	12	No CF	No CF
46	3/11/79	11:26	17057	47N/165W	22	8	Yes CF	Yes CF
47	11/11/81	1226Z	15399	38N/177E	54	12	Yes WF + L	Yes WF + L
48	11/13/81	0937Z	15425	37N/145W	36	12	Yes CF	Yes CF

Key for the symbols:

CF for "Cold Front"
WF for "Warm Front"
J for "Junction of storm"
L for "Low"
DW for "Developing Wave"
OF for "Old Front"
OC for "Occluded"

No	Sketch of SMMR Swath	Qualitative Assessment
39		Some rain interference near OF and at Low, otherwise strong signal in pattern. Old CF has very high vapor amounts. GOOD
40		Two frontal systems. The eastern front has highest vapor. Gradient continues to behind second front, so that there is no secondary max. at western front. Warm front not easily distinguished. GOOD
41		Strong gradient behind the cold front. A typical convincing case. V. GOOD
42	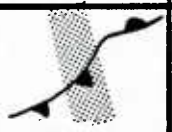	A typical case of strong gradient behind CF. Max. ahead of the front. GOOD
43	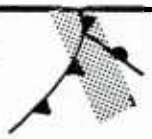	Inverted V shape in max moisture dist. Grad weak-mod. Some rain along all fronts GOOD
44		Very weak system, max very narrow in small blobs near front. Field looks flat. OK
45		Max in large broad area, gradient strong right at front, otherwise looks flat. OK
46		CF along max and gradients are both to N and S. Low in region of minor max. GOOD
47	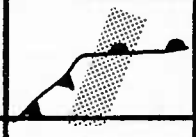	Broad region of very high vapor content. Max along WF. GOOD
48		Low center coincident with local minimum. Maximum along CF, strong gradient, especially to the south. V. GOOD

Continued

APPENDIX B:

CYCLONIC STORMS STUDIED WITH SMMR DATA.

No	Date	Time GMT	Rev.#	Center of swath Lat/Lon	Max. Vapor Kg/m²	Min. Vapor kg/m²	WV Flag Catches	Rain Signal Catches
49	11/13/81	1933Z	15431	40N/127W	32	17	Yes CF	Yes CF + L
RAPIDLY DEVELOPING CYCLONES (SANDER'S BOMBS)								
50	01/03/81	03:50	11082	43N/54W	36	12	Yes CF	Yes CF
51	01/09/81	03:59	11165	42N/57W	36	12	Yes CF	Yes CF
52	01/09/81	13:57	11171	45N/42W	24 28	10	Yes CF Yes CF	Yes CF Yes CF
53	01/17/81	04:51	11276	30N/70W	32	8	Yes CF	Yes CF
54	01/17/81	14:41	11282	37N/52W	44	12	Yes CF + L	Yes CF + L
55	01/17/81	16:27	11283	30N/75W	32	12	Yes CF	Yes CF
56	03/06/81	04:11	11939	30N/60W	32	12	Yes WF	Yes CF
57	03/06/81	15:47	11946	31N/65W	36	14	Yes CF	Yes CF + L
58	09/20/81	05:03	14676	35N/72W	55	20	Yes CF	Yes CF

Key for the symbols:

CF for "Cold Front"
WF for "Warm Front"
J for "Junction of storm"
L for "Low"
DW for "Developing Wave"
OF for "Old Front"
OC for "Occluded"

No	Sketch of SMMR Swath	Qualitative Assessment
49		Sampled east of storm. Maximum near WF. OK
		RAPIDLY DEVELOPING CYCLONES (Sander's Bombs)
50		Strong gradient behind CF. Max. along front, A typical case. GOOD - V. GOOD
51		Gradient parallel to the CF. Max. ahead and south of CF. GOOD
52		Two frontal systems sampled. Gradient is moderately stronger at the DW than at the occluded front. OK
53	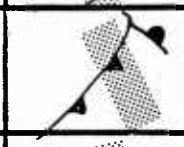	Two mature frontal systems sampled. Max. WV values at the tail end of CF. Gradient is strong close to Low. GOOD
54		Gradient stronger close to Low than at the CF. But the vapor values higher behind the the CF. OK
55	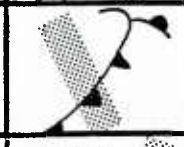	A typical case of strong gradient at the leading edge of CF. GOOD
56		Strong gradient ahead of WF. Max. vapor values the south of WF. GOOD
57	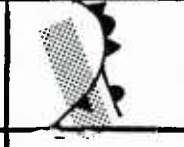	A typical case with strong gradient behind CF. Pattern agrees with SMMR analysis. GOOD
58		Very strong gradient behind the end tail of CF. Max lies at the front. V. GOOD

Continued

APPENDIX B:

CYCLONIC STORMS STUDIED WITH SMMR DATA.

No	Date	Time GMT	Rev.#	Center of swath Lat/Lon	Max. Vapor Kg/m²	Min. Vapor kg/m²	WV Flag Catches	Rain Signal Catches
59	09/20/81	14:56	14682	35N/55W	46	16	Yes CF + L	Yes CF + L
60	09/26/81	03:24	14758	40N/46W	44	16	Yes CF	Yes CF + WF
61	09/26/81	13:23	14764	45N/34W	40	12	Yes WF	Yes WF
62	09/26/81	15:06	14765	40N/60W	44	12	Yes CF	Yes CF
63	11/25/81	04:44	15588	26N/70W	28 50	12 19	Yes CF Yes CF	Yes CF No CF
64	11/25/81	16:16	15595	26N/72W	44	17	Yes CF	No CF
65	12/05/81	15:56	15733	26N/67W	38	17	Yes CF	Yes CF + L

Key for the symbols:

CF for "Cold Front"
WF for "Warm Front"
J for "Junction of storm"
L for "Low"
DW for "Developing Wave"
OF for "Old Front"
OC for "Occluded"

No	Sketch of SMMR Swath	Qualitative Assessment
59		Few blobs of higher moisture ahead of main system are perhaps due to convective clouds. Otherwise strong gradient pattern behind the CF is a normal case. V. GOOD
60		Another good case of agreement with the hypothesis. V. GOOD
61		WV vapor contours do align parallel to the WF and show strong gradient. Max lies south of the WF. OK
62		Max. lies at the CF. Strong gradient behind the CF. GOOD
63	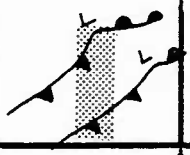	Two frontal systems sampled. Gradient is stronger at the southern system than at the northern one. Gradient pattern does correlate with both systems. GOOD
64	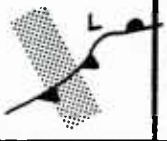	Rather odd water vapor pattern, with very strong gradient. Perhaps two CFs close to each other are causing this strange pattern. Otherwise looks good. GOOD
65		A trof and CF are close to each other. Max. lies at the trof. A typical case. GOOD

DISTRIBUTION

ASST. FOR ENV. SCIENCES
ASST. SEC. OF THE NAVY (R&D)
ROOM 5E731, THE PENTAGON
WASHINGTON, DC 20350

OFFICE OF NAVAL RESEARCH
CODE 1122AT, ATMOS. SCIENCES
ARLINGTON, VA 22217-5000

OFFICE OF NAVAL RESEARCH
ATTN: HEAD, OCEAN SCIENCES DIV
CODE 1122
ARLINGTON, VA 22217-5000

CHIEF OF NAVAL OPERATIONS
OP-962
U.S. NAVAL OBSERVATORY
WASHINGTON, DC 20390

OFFICER IN CHARGE
NAVOCEANCOMDET
NAVAL EDUCATION & TRNG CENTER
NEWPORT, RI 02841-5000

COMMANDING OFFICER
NAVAL RESEARCH LAB
ATTN: LIBRARY, CODE 2620
WASHINGTON, DC 20390

COMMANDING OFFICER
OFFICE OF NAVAL RESEARCH
1030 E. GREEN ST.
PASADENA, CA 91101

OFFICE OF NAVAL RESEARCH
SCRIPPS INSTITUTION OF
OCEANOGRAPHY
LA JOLLA, CA 92037

COMMANDING OFFICER
NAVAL OCEAN RSCH & DEV ACT
NSTL, MS 39529-5004

COMNAVOCEANCOM
ATTN: CODE N5
NSTL, MS 39529-5000

COMMANDING OFFICER
NAVAL OCEANOGRAPHIC OFFICE
BAY ST. LOUIS
NSTL, MS 39522-5001

COMMANDING OFFICER
NAVPOLAROCEANCEN, NAVY DEPT.
4301 SUITLAND RD
WASHINGTON, DC 20395-5180

SUPERINTENDENT
LIBRARY REPORTS
U.S. NAVAL ACADEMY
ANNAPOLIS, MD 21402

CHAIRMAN
OCEANOGRAPHY DEPT.
U.S. NAVAL ACADEMY
ANNAPOLIS, MD 21402

DIRECTOR OF RESEARCH
U.S. NAVAL ACADEMY
ANNAPOLIS, MD 21402

NAVAL POSTGRADUATE SCHOOL
METEOROLOGY DEPT.
MONTEREY, CA 93943-5000

NAVAL POSTGRADUATE SCHOOL
OCEANOGRAPHY DEPT.
MONTEREY, CA 93943-5000

LIBRARY
NAVAL POSTGRADUATE SCHOOL
MONTEREY, CA 93943-5002

COMMANDER (2)
NAVAIRSYSCOM
ATTN: LIBRARY (AIR-723D)
WASHINGTON, DC 20361-0001

COMMANDER
NAVAIRSYSCOM, CODE 526W
WASHINGTON, DC 20361-0001

COMSPAWARSYSCOM
ATTN: CAPT. R. PLANTE
CODE 3213, NAVY DEPT.
WASHINGTON, DC 20363-5100

COMSPAWARSYSCOM
ATTN: CODE PMW 141-B1
WASHINGTON, DC 20363-5100

COMMANDER
PACMISTESTCEN
GEOPHYSICS OFFICER
PT. MUGU, CA 93042

USAFETAC/TS
SCOTT AFB, IL 62225

AFGWC/DAPL
OFFUTT AFB, NE 68113

AFGL/LY
HANSCOM AFB, MA 01731

DIRECTOR (12)
DEFENSE TECH. INFORMATION
CENTER, CAMERON STATION
ALEXANDRIA, VA 22314

DIRECTOR
NATIONAL HURRICANE CENTER
NOAA, GABLES ONE TOWER
1320 S. DIXIE HWY
CORAL GABLES, FL 33146

LIBRARY ACQUISITIONS
NCAR, P.O BOX 3000
BOULDER, CO 80307

HEAD, ATMOS. SCIENCES DIV.
NATIONAL SCIENCE FOUNDATION
1800 G STREET, NW
WASHINGTON, DC 20550

EXECUTIVE SECRETARY, CAO
SUBCOMMITTEE ON ATMOS. SCI.
NATIONAL SCIENCE FOUNDATION
RM. 510, 1800 G. STREET, NW
WASHINGTON, DC 20550

COLORADO STATE UNIVERSITY
ATMOSPHERIC SCIENCES DEPT.
ATTN: DR. WILLIAM GRAY
FORT COLLINS, CO 80523

CHAIRMAN
INSTITUTE OF ATMOS. PHYSICS
UNIV. OF ARIZONA
TUSCON, AZ 85721

SCRIPPS INSTITUTION OF
OCEANOGRAPHY, LIBRARY
DOCUMENTS/REPORTS SECTION
LA JOLLA, CA 92037

WOODS HOLE OCEANO. INST.
DOCUMENT LIBRARY LO-206
WOODS HOLE, MA 02543

COLORADO STATE UNIVERSITY
ATMOSPHERIC SCIENCES DEPT.
ATTN: LIBRARIAN
FT. COLLINS, CO 80523

UNIVERSITY OF WASHINGTON
ATMOSPHERIC SCIENCES DEPT.
SEATTLE, WA 98195

CHAIRMAN, METEOROLOGY DEPT.
PENNSYLVANIA STATE UNIV.
503 DEIKE BLDG.
UNIVERSITY PARK, PA 16802

UNIVERSITY OF HAWAII
METEOROLOGY DEPT.
2525 CORREA ROAD
HONOLULU, HI 96822

DIRECTOR
COASTAL STUDIES INSTITUTE
LOUISIANA STATE UNIVERSITY
ATTN: O. HUH
BATON ROUGE, LA 70803

MR. W. G. SCHRAMM/WWW
WORLD METEOROLOGICAL
ORGANIZATION
CASE POSTALE #5, CH-1211
GENEVA, SWITZERLAND

METEORO. OFFICE LIBRARY
LONDON ROAD
BRACKNELL, BERKSHIRE
RG 12 1SZ, ENGLAND